Precambrian Research 260 (2015) 76–90

Contents lists available at ScienceDirect

Precambrian Research

journal homepage: www.elsevier.com/locate/precamres

Provenance and depositional age of Paleoproterozoic metasedimentary rocks in the Kuluketage Block, northern Tarim Craton: Implications for tectonic setting and crustal growth

Xiaoping Long[a,*], Simon A. Wilde[b], Chao Yuan[a], Aiqin Hu[a], Min Sun[c]

[a] Key Laboratory of Isotope Geochronology and Geochemistry, Guangzhou Institute of Geochemistry, Chinese Academy of Sciences, Guangzhou, China
[b] Department of Applied Geology, Curtin University of Technology, Perth, WA 6845, Australia
[c] Department of Earth Sciences, The University of Hong Kong, Pokfulam Road, Hong Kong, China

ARTICLE INFO

Article history:
Received 22 June 2014
Received in revised form 13 January 2015
Accepted 21 January 2015
Available online 30 January 2015

Keywords:
Xingditage Group
Provenance
Basement
Crustal growth
Tarim Craton

ABSTRACT

Precambrian geology of the Tarim Craton, especially for the crustal evolution, is poorly constrained. Paleoproterozoic metasedimentary rocks are extensively exposed in the Kuluketage Block, northern Tarim Craton, and thus have recorded abundant geological information of its tectonic history. Supracrustal rocks within the Archean basement (Tuoge Complex) and the Paleoproterozoic Xingditage Group were collected from the Kuluketage Block for geochemical study and zircon U–Pb dating. The Tuoge supracrustal rocks have low CIA values between 45 and 63, indicating weak chemical weathering. Although the Xingditage Group shows a large variation of CIA values (37–67), their low average value suggests that they underwent similar weathering to the rocks from the basement. This similarity is also supported by their respective PIA values (mostly 43–57 for the basement rocks, and mostly 37–60 for the Xingditage Group). The high ICV values (mostly >1) of both rock suites indicate an immature source that lacked alumina-rich minerals. Although these metasedimentary rocks show different REE patterns, they are all enriched in light rare earth element (LREE) and display relatively flat heavy rare earth element (HREE) patterns. The low values of ferromagnesian (e.g. Cr, Co and Ni) and high field strength elements (e.g. Zr, Hf, Nb, Ta and Y) are similar to those of graywackes from active continental margins. Therefore, the Kuluketage Block most likely evolved in an active continental margin setting during the late Paleoproterozoic. Detrital zircons from a slate sample of the Tuoge supracrustal rocks are dominated by igneous zircons, which mostly yield Paleoproterozoic $^{207}Pb/^{206}Pb$ ages between 1.72 Ga and 2.08 Ga. Other igneous grains give Paleoproterozoic $^{207}Pb/^{206}Pb$ ages at ~2.2 Ga and ~2.32 Ga. All these igneous zircons show large variations of $\varepsilon_{Hf}(t)$ values mostly between −17 and −3, and have Neoarchean crustal model ages (T_{DM}^{c} = 2.6–3.7 Ga). Schist and quartzite samples of the upper Xingditage Group show similar age spectra to the slate and contain a major igneous zircon population with Paleoproterozoic formation ages (mostly 1.8–2.1 Ga) and Paleo- to Mesoarchean T_{DM}^{c} ages (2.7–3.1 Ga). A schist sample of the lower Xingditage Group shows a much different age spectrum. Detrital zircons from this sample are dominated by Neoarchean grains (2.5–2.7 Ga) with Paleoarchean T_{DM}^{c} ages (3.14–3.51 Ga) and two of them yield the youngest ages at 1.94 and 2.09 Ga. The youngest zircons from these samples, therefore, define the maximum depositional ages at 1.63, 1.94 and 1.77 Ga for the Tuoge supracrustal rocks, the upper Xingditage Group and the lower Xingditage Group, respectively. On basis of these age spectra, we suggest that the Tuoge supracrustal rocks are equivalents of the upper Xingditage Group, instead of parts of the Archean basement. Overall, the Hf isotopic compositions of these detrital zircons indicate three early Precambrian crustal growth events in the Tarim Craton, which occurred in the late Paleoarchean, the early Neoarchean and at the beginning of the Paleoproterozoic.

1. Introduction

Episodic magmatism is a most striking feature of cratons and continents (Stein and Hofmann, 1994; Condie, 1998), and records the major geological events, such as the assembly and breakup of

* Corresponding author. Tel.: +86 20 8529 0907.
E-mail address: longxp@gig.ac.cn (X. Long).

http://dx.doi.org/10.1016/j.precamres.2015.01.008
0301-9268/

supercontinent and the formation of plume (Condie, 1998, 2000). Several age peaks of magmatism that has been widely recognized and well documented by recent high-precision U–Pb and Hf isotopic studies of zircons (Condie, 2000, Condie et al., 2011; Wang et al., 2009; Yang et al., 2009). In the early Precambrian, the major episodes were identified at 3.3, 2.7, 2.68, 2.5, 2.1, 1.9 and 1.1 Ga for magmatic rocks of main cratons, but 2.78, 2.7, 2.6, 2.5, 1.9, 1.65 and 1.2 Ga for detrital zircons from sediments of modern large rivers (Condie et al., 2009; and references therein). These peaks are totally considered as the time of crustal growth or reworking, although some of them are different in the two series studies. However, the age peaks obtained by zircon U–Pb dating and Hf isotopic analyses are partial inconsistent with the Nd isotope distributions that suggest important additions of juvenile continental crust at 2.7, 2.5, 2.1, 1.9, 1.7 and 1.65 Ga (Condie et al., 2009, 2011). Thus, it is still unclear whether the each episodic magmatism was dominated by juvenile crustal growth or reworking of ancient crustal material.

The Tarim Craton is located in Northwestern China and covered by huge Cenozoic deposits in its central part (Hu et al., 2000; Lu et al., 2008; Zhao and Cawood, 2012). Precambrian basement rocks were dominantly exposed in several small blocks surrounding the Tarim Basin, including the Kuluketage, Northern Altny Tagh, Akesu and Tiekelike blocks (Fig. 1; BGMRX, 1993). Recently, Archean basement rocks have been identified mainly in the Kuluketage and the Northern Altny Tagh blocks, where they are overlain by the Paleo- to Neoproterozoic metasedimentary rocks (Hu et al., 1997, 2000; Lu et al., 2008). Zircon U–Pb dating of the Archean rocks yielded Neoarchean ages between 2.5 and 2.8 Ga, with peaks at ~2.55 and ~2.71 Ga (Lu and Yuan, 2003; Lu et al., 2008; Long et al., 2010, 2011a, 2014; Liu et al., 2010; Shu et al., 2011; Zhang et al., 2012a, 2013a, 2013b, 2014; Zong et al., 2013; Ge et al., 2014a, 2014b). In the Kuluketage, Long et al. (2010) firstly recognized a ~2.55 Ga magmatism of crustal reworking and a juvenile crustal growth in the latest Neoarchean (~2.5 Ga) after the identification of Archean basement rocks. Then, based on zircon Hf–O isotopic studies, Ge et al. (2014a, 2014b) defined another magmatism at ~2.7 Ga and suggested that the two peaks of magmatism (~2.55 and ~2.7 Ga) do not represent the time of crustal growth but are artifacts of magma mixing. They proposed that there are significant amounts of felsic continental crust formed before 3.5 Ga. In the Northern Altny Tagh, Zong et al. (2013) suggested that the two peaks have recorded the reworking of older crust and episodic crustal growths of the Tarim Craton occurred at ~3.4, ~3.2, ~2.95, ~2.8 and ~2.6 Ga. In contract, Long et al. (2014) considered that the two periods of magmatism are characterized by juvenile crust formation with variable crustal reworking. However, Zhang et al. (2014) argued that continental growth in this area took place since 4.3 Ga. These different recognitions on the crustal growth or reworking, therefore, have hampered a better understanding of the tectonic evolution of the Tarim Craton in the early Precambrian.

Compared to the sparsely exposed Archean basement, Proterozoic metasedimentary rocks are extensively distributed in the blocks surrounding the Tarim Basin but have been poorly studied (Long et al., 2010; Shu et al., 2011; Ge et al., 2013). The Proterozoic metasediments were transported from an older source, including the Archean basement, and thus can shed light on the crustal evolution of the Tarim Craton. In order to provide close constraints on the process of the crustal growth and reworking, we present whole-rock geochemistry, zircon U–Pb and Hf isotopic data for the Paleoproterozoic Xingditage Group in the Kuluketage Block, northern Tarim Craton. Together with similar studies on supracrustal rocks exposed within the Archean basement, we define three early Precambrian crustal growth events in the Tarim Craton and suggest an active continental margin for the northern Tarim Craton when the Xingditage Group deposited.

2. Geological background

The Tarim Craton is located in Northwest China and surrounded by the Tianshan orogen to the north, the western Kunlun orogen to the south, and the Altyn Tagh orogen to the southeast (Fig. 1, inset). Precambrian basement rocks are only exposed along the craton margins exposed around the Tarim Basin, e.g. the Kuluketage Block (also named “Quruqtagh” in the literature) in the northeast, the Aksu Block in the northwest, the Tiekelike Block in the southwest and the Dunhuang Block in the east (BGMRX, 1993; Hu et al., 2000; Lu and Yuan, 2003; Guo et al., 2003, 2005; Xu et al., 2005, 2009; Lu et al., 2008; Zhang et al., 2007a, 2007b, 2009, 2011, 2012a; Long et al., 2010, 2011a; Long et al., 2011b, 2012a; Shu et al., 2011; Cao et al., 2011; Ge et al., 2012, 2014a, 2014b; Zhu et al., 2011a, 2011b; He et al., 2012; Zhang et al., 2012b, 2013b, 2014). Archean rocks from the Precambrian basement consist predominantly of strongly deformed tonalitic–trondhjemitic–granodioritic (TTG) orthogneisses and metamorphosed supracrustal xenoliths, sparsely exposed in the Kuluketage and Dunhuang blocks along the northern and eastern margins of the craton (Zhao and Cawood, 2012 and references therein). The Archean basement rocks have commonly undergone medium- to high-grade metamorphism (BGMRX, 1993; Hu et al., 2000; Lu et al., 2008).

The Kuluketage Block is situated between the Southern Tianshan Range to the north and the Tarim Basin to the south (Fig. 1). In this area, the early Precambrian rocks are known as the Tuoge Complex, which are the oldest basement rocks, unconformably overlain by the Paleoproterozoic Xinditage Group (Gao et al., 1993; BGMRX, 1993; Hu et al., 1997, 2000). The complex consists predominantly of high-grade metamorphic TTG and supracrustal rocks (BGMRX, 1993; Hu et al., 2000; Guo et al., 2003). The TTG rocks are Na-enriched and composed of gray gneissic tonalite and granitoid (Hu et al., 1997). Recent zircon dating of the TTG rocks indicates that these rocks were mainly emplaced during the period of 2.65–2.50 Ga (Long et al., 2010, 2011a; Shu et al., 2011; Zhang et al., 2012a). Some calc-alkaline and high Ba–Sr granites also occur in the area and yielded Neoarchean emplacement ages (~2.53 Ga, Zhang et al., 2012a). The supracrustal rocks mainly consist of lenses of amphibolite and sedimentary sequence, which is an association of interlayered intermediate-mafic volcanic and clastic sedimentary rocks within the TTG gneisses (Gao et al., 1993; Guo et al., 2003). Unconformably overlying the Tuoge Complex, Proterozoic metasedimentary rocks are well exposed in the Kuluketage area (Fig. 1) and have experienced two respective metamorphic events at 1.9–1.8 Ga and 1.1–1.0 Ga, which are inferred to have a relationship with the assembly of the Columbia (Nuna) and Rodinia supercontinents, respectively (Shu et al., 2011; Long et al., 2012a; Zhang et al., 2007b, 2009, 2012a, 2012b; Ge et al., 2013).

The Paleoproterozoic Xingditage Group and the Mesoproterozoic Aierjigan Group are typical marine sedimentary sequences consisting of clastic and carbonate rocks, covered by Neoproterozoic marine sediments (BGMRX, 1993; Gao et al., 1993; Hu et al., 1997; Lu et al., 2008). These rocks show a consistent NW–SE trend, with upright to steeply south-dipping regional foliations. They are locally intruded by late Neoproterozoic and early Paleozoic igneous rocks (Long et al., 2010; Zhu et al., 2011b; Ge et al., 2012, 2013). Paleoproterozoic granites also occur locally near Korla and Xinger (Fig. 2a). These rocks yield ages between 1.91 Ga and 1.94 Ga and are considered to be associated with the assembly of the Columbia supercontinent (Zhang et al., 2007a, 2013b; Shu et al., 2011; Zhu et al., 2011b; Lei et al., 2012; Long et al., 2012a; Ge et al., 2013; Wu et al., 2014).

Ten samples, including four mica schists and six slates, were collected from the Tuoge supercrustal rocks south to Xinger (Fig. 2a) for geochemical study, together with seventeen schist samples

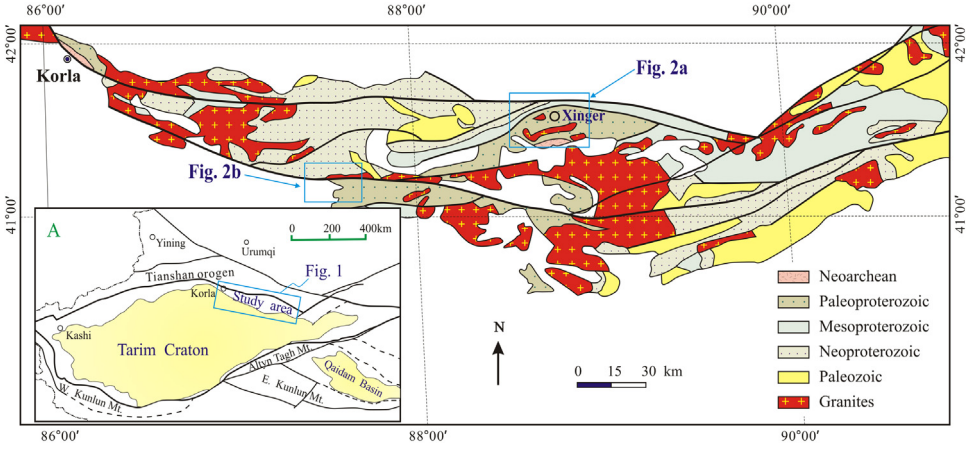

Fig. 1. Simplified geological map of the Kuluketage Block, northern Tarim Craton (after Long et al., 2010). Inset: an outline of the Tarim Craton and adjacent areas (after Lu et al., 2008).

from the Xingditage Group exposed in the southern Kuluketage Block (Fig. 2b). In the two studied sections, the sedimentary rocks are mostly low-grade metamorphosed and slightly deformed. They were intruded by Paleoproterozoic and Neoproterozoic deformed granites in the Xinger section and Xingdi section, respectively. The Xingditage schists are composed of recrystallized quartz and plagioclase, with biotite defining the schistosity (Fig. 3a and c). In some schist samples, a mineral association of kyanite and silimanite indicate amphibolite facies metamorphism (Fig. 3d). The slate samples from the Tuoge supercrustal rocks are fine-grained and mainly consist of quartz and plagioclase, with minor biotite (Fig. 3b). In addition, one slate from the Tuoge supercrustal rocks, two schists and one quartzite from the overlying Xingditage Group were collected for zircon U–Pb dating and Hf isotopic analysis (Fig. 2).

3. Analytical methods

3.1. Major and trace elements

Thirty-three samples chosen for elemental and isotopic analysis were crushed to small pieces, ultrasonically cleaned in distilled water, then dried and powdered to 0.074 mm. Major element oxides were determined on fused discs with a 1:8 sample to $Li_2B_4O_7$ flux ratio, using a Rigaku ZSX100e X-ray fluorescence spectrometer at the Key Laboratory of Isotope Geochronology and Geochemistry, Guangzhou Institute of Geochemistry, Chinese Academy of Sciences. The precision of the XRF analyses is estimated as ca. 1% for SiO_2, ca. 5% for MnO and P_2O_5 and ca. 2% for other major oxides. The analytical procedures are described by Yuan et al. (2010). Trace elements, including the rare earth elements (REE), were analyzed using a Perkin-Elmer Sciex ELAN 6000 ICP-MS at the Guangzhou Institute of Geochemistry, Chinese Academy of Sciences. The powdered samples (50 mg) were digested with mixed HNO_3 + HF acid in Teflon-coated steel bombs in order to assure complete dissolution of refractory minerals. An internal standard solution containing Rh was used to monitor the signal drift. The USGS rock standards G-2, W-2, MRG-1 and AGV-1, and the Chinese national rock standards GSD-12, GSR-1, GSR-2 and GSR-3, were analyzed to calibrate the elemental concentrations of the measured samples. The obtained analytical precision was generally better than 5% for all trace elements. Sample preparation techniques and other details were described by Long et al. (2012b) and Huang et al. (2013). Major and trace element results are listed in Table 1 .

3.2. Zircon U–Pb dating and Hf-in-zircon isotopic analysis

Five samples were prepared for zircon analysis using heavy liquid and magnetic techniques and then by handpicking under a binocular microscope. Zircon grains were mounted on adhesive

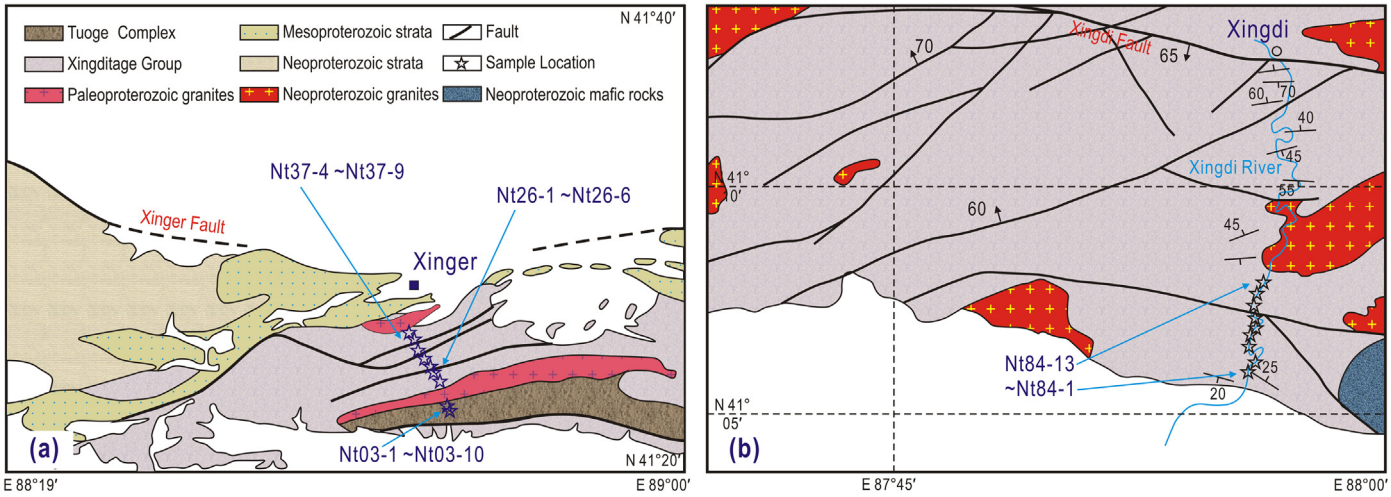

Fig. 2. Geological map of the central (a) and southern (b) Kuluketage Block, northern Tarim Craton.

Table 1
Geochemistry of Paleoproterozoic metasedimentary rocks in the Kuluketage Block, northern Tarim Craton.

Sample	Nt03-1	Nt03-2	Nt03-9	Nt03-5	Nt03-3	Nt03-4	Nt03-6	Nt03-7	Nt03-8	Nt03-10	PAAS
	Mica Schist				Slate						Shale
SiO_2	69.48	64.55	67.45	60.83	81.61	73.54	80.67	71.62	82.47	73.46	62.8
TiO_2	0.33	0.49	0.48	0.73	0.19	0.37	0.31	0.33	0.22	0.08	1
Al_2O_3	15.45	11.24	15.59	18.06	9.12	12.69	9.62	12.03	8.44	15.16	18.9
Fe_2O_3	2.31	3.58	4.24	5.80	1.75	4.12	2.17	2.07	2.71	0.63	6.5
MnO	0.04	0.07	0.08	0.06	0.05	0.11	0.07	0.07	0.05	0.04	0.11
MgO	1.29	3.28	1.52	2.07	0.91	1.23	0.59	3.34	0.87	0.33	2.2
CaO	1.55	5.19	2.77	3.00	1.90	2.09	1.72	2.40	0.16	1.73	1.3
Na_2O	4.02	0.12	4.34	3.66	2.17	3.37	2.46	1.98	0.89	4.58	1.2
K_2O	2.58	3.51	1.89	3.95	1.04	1.23	1.38	4.33	2.87	2.80	3.7
P_2O_5	0.04	0.16	0.11	0.09	0.07	0.08	0.07	0.11	0.04	0.03	0.16
L.O.I	2.81	8.33	1.40	1.66	0.93	0.97	0.68	1.59	1.03	0.98	
Total	99.90	100.52	99.87	99.93	99.76	99.81	99.75	99.86	99.75	99.81	97.9
CIA	56	45	52	53	53	54	53	49	63	52	69
PIA	57	43	53	55	53	55	53	49	75	53	77
ICV	0.78	1.44	0.98	1.07	0.88	0.99	0.90	1.21	0.92	0.67	0.84
Sc	4.16	11.3	4.34	13.4	2.23	6.63	4.99	5.27	2.64	0.83	16
Cr	64.7	84.3	14.4	90.3	22.1	54.8	35.6	42.7	16.5	15.1	110
Co	3.71	6.51	10.5	9.16	4.30	8.80	4.05	3.27	6.05	1.11	
Ni	11.0	20.6	17.9	21.5	9.05	27.0	11.6	12.7	8.43	3.25	55
Rb	66.5	138	49.8	149	33.8	49.7	51.9	123	72.2	42.1	160
Sr	308	308	455	308	229	328	212	136	30.5	601	200
Ba	1435	460	876	1716	213	247	645	1033	729	2235	650
Zr	79.0	129	131	515	147	117	172	238	168	46.4	210
Hf	2.09	3.20	3.01	10.5	3.38	3.00	4.03	6.30	4.64	1.19	5
Y	2.83	12.9	5.16	43.1	8.84	19.3	17.3	16.7	22.5	4.16	27
Nb	3.63	7.82	2.93	17.2	4.70	8.11	8.18	9.14	4.45	1.34	19
Ta	0.23	0.63	0.11	0.84	0.74	0.76	0.53	0.82	0.13	0.11	1.28
Pb	6.98	13.9	48.0	18.7	21.3	33.0	14.9	32.7	10.6	47.5	20
Th	1.33	8.31	7.08	21.0	4.44	6.85	8.70	13.6	18.9	1.08	14.6
U	0.43	3.15	0.41	2.18	0.98	1.06	1.46	2.24	0.64	0.30	3.1
La	9.92	14.7	31.8	81.0	13.5	20.6	34.4	10.5	61.8	7.29	38.2
Ce	18.7	30.5	60.5	173	28.3	42.9	70.4	21.6	124	14.5	79.6
Pr	2.17	3.58	7.12	21.2	3.50	5.12	8.54	2.65	14.9	1.68	8.83
Nd	7.41	12.3	23.0	72.1	12.0	17.9	28.9	9.40	47.5	5.75	33.9
Sm	1.20	2.27	3.00	11.8	2.20	3.19	4.59	1.91	7.83	1.05	5.55
Eu	0.52	0.58	0.73	1.71	0.48	0.75	0.68	0.33	0.74	0.44	1.08
Gd	1.04	2.04	2.11	9.23	1.78	2.74	3.64	2.03	6.28	0.91	4.66
Tb	0.13	0.31	0.21	1.25	0.27	0.44	0.48	0.39	0.87	0.12	0.774
Dy	0.55	1.86	0.97	7.05	1.49	2.87	2.68	2.68	4.38	0.65	4.68
Ho	0.09	0.39	0.17	1.42	0.28	0.61	0.53	0.60	0.76	0.13	0.991
Er	0.24	1.17	0.40	3.89	0.76	1.72	1.51	1.66	1.82	0.36	2.85
Tm	0.03	0.18	0.05	0.56	0.12	0.27	0.24	0.27	0.24	0.06	0.405
Yb	0.25	1.28	0.36	3.56	0.78	1.77	1.63	1.83	1.44	0.40	2.82
Lu	0.04	0.20	0.06	0.51	0.12	0.26	0.26	0.28	0.21	0.07	0.433
$(La/Yb)_N$	28	8	63	16	12	8	15	4	31	13	9.72
$(Gd/Yb)_N$	3.4	1.3	4.9	2.1	1.9	1.3	1.8	0.9	3.6	1.9	1.37
Eu/Eu*	1.43	0.83	0.89	0.51	0.75	0.78	0.51	0.52	0.33	1.38	0.63
$\sum$REE	42	71	130	388	65	101	158	56	272	33	185

Sample	Nt26-1	Nt26-2	Nt26-3	Nt26-4	Nt26-6	Nt37-4	Nt37-5	Nt37-9	Nt84-1	Nt84-2	Nt84-3	Nt84-4	Nt84-6	Nt84-7	Nt84-10	Nt84-12	Nt84-13
	Mica Schist from the central Kuluketage Block								Mica Schist from the northern Kuluketage Block								
	Xingditage Group								Xingditage Group								
SiO_2	58.44	59.53	61.23	76.63	61.55	67.25	67.76	64.01	52.86	55.26	58.23	56.38	61.60	60.09	61.13	58.20	60.44
TiO_2	0.45	0.46	0.31	0.20	0.29	0.52	0.56	0.61	0.93	0.69	1.28	1.66	1.11	1.51	1.10	1.62	0.96
Al_2O_3	17.93	18.28	17.23	6.96	16.86	10.12	10.44	11.63	13.74	14.10	17.25	16.43	16.57	15.26	14.71	15.12	16.26
Fe_2O_3	5.22	4.98	3.52	3.90	2.70	4.21	3.97	4.80	8.24	7.15	7.37	11.25	7.87	9.33	8.32	9.66	8.19
MnO	0.10	0.10	0.10	0.10	0.06	0.15	0.13	0.14	0.14	0.12	0.08	0.09	0.08	0.08	0.07	0.08	0.07
MgO	1.05	1.12	0.99	1.66	2.26	1.89	1.32	2.68	8.76	9.04	3.97	3.71	3.10	4.15	4.32	4.51	4.17
CaO	3.56	4.79	3.61	3.41	3.56	5.44	5.49	5.32	7.52	6.61	3.25	1.35	0.80	1.22	2.60	2.76	1.20
Na_2O	4.18	3.79	4.33	0.08	0.33	2.85	4.22	2.07	2.43	3.15	2.40	1.81	0.90	1.05	1.49	1.80	1.54
K_2O	4.34	3.47	3.93	2.98	6.67	1.18	0.49	2.24	3.19	2.20	3.25	4.92	4.87	4.74	3.73	4.23	4.86
P_2O_5	0.17	0.18	0.13	0.08	0.13	0.14	0.13	0.18	0.41	0.22	0.16	0.24	0.10	0.15	0.14	0.17	0.06
L.O.I	4.30	2.95	4.32	3.71	5.51	6.23	5.35	6.34	1.35	1.00	2.37	1.74	2.64	2.03	2.00	1.40	1.83
Total	99.75	99.65	99.69	99.72	99.91	99.98	99.86	100.02	99.56	99.56	99.62	99.59	99.64	99.61	99.61	99.57	99.57
CIA	50	49	49	42	54	39	37	43	39	42	56	60	67	63	57	55	62
PIA	50	49	49	37	58	38	37	41	37	40	58	67	79	72	60	57	70
ICV	1.05	1.02	0.97	1.77	0.94	1.60	1.55	1.54	2.27	2.05	1.25	1.51	1.13	1.45	1.47	1.63	1.29
Sc	10.5	10.6	10.2	11.6	8.32	13.5	14.2	16.7	29.2	25.0	21.8	29.6	24.2	22.3	18.4	21.6	24.7
Cr	59.5	61.0	56.2	84.4	36.6	136	137	125	567	779	106	191	195	95.7	94.8	89.5	155
Co	3.48	7.14	8.06	2.43	3.56	12.6	12.9	12.5	51.0	47.3	16.6	40.4	22.6	19.2	16.0	16.6	22.8
Ni	14.3	13.8	16.4	14.9	8.55	40.7	41.9	41.4	257	344	50.2	96.1	76.7	35.2	39.9	28.8	55.0
Rb	105	81.5	90.4	90.9	167	44.7	10.6	92.6	99.4	87.8	150	257	248	220	189	197	285

Table 1 (*Continued.*)

Sample	Nt26-1	Nt26-2	Nt26-3	Nt26-4	Nt26-6	Nt37-4	Nt37-5	Nt37-9	Nt84-1	Nt84-2	Nt84-3	Nt84-4	Nt84-6	Nt84-7	Nt84-10	Nt84-12	Nt84-13
	Mica Schist from the central Kuluketage Block								Mica Schist from the northern Kuluketage Block								
	Xingditage Group								Xingditage Group								
Sr	351	1183	237	152	119	198	166	173	951	988	208	222	134	81.2	171	148	149
Ba	1274	1525	1694	1448	3636	448	292	698	1751	1021	718	1067	894	549	536	515	800
Zr	162	138	167	224	205	216	233	260	145	126	224	293	308	175	138	240	204
Hf	4.43	3.60	4.26	5.71	5.02	5.45	5.88	6.61	3.89	3.23	6.11	7.58	7.97	4.58	3.63	6.44	5.44
Y	19.8	21.1	19.3	11.4	13.5	24.0	22.8	26.6	20.4	14.1	21.7	30.1	24.0	11.3	16.6	14.7	18.2
Nb	9.57	8.81	7.91	5.40	10.3	10.0	10.5	12.3	12.2	5.41	24.5	37.0	31.4	23.1	16.1	33.1	24.8
Ta	0.63	0.58	0.49	0.40	0.59	0.74	0.77	0.90	0.97	0.31	1.62	2.53	2.11	1.56	1.13	2.34	1.94
Pb	9.61	15.8	11.6	10.9	9.07	13.9	2.64	12.6	15.8	16.0	25.9	21.1	22.2	14.1	15.3	13.1	26.7
Th	5.74	5.43	4.73	8.92	5.86	8.16	8.52	9.25	4.11	2.04	14.2	15.1	16.1	9.35	10.9	9.77	16.5
U	1.00	1.35	0.93	0.76	1.58	1.89	2.81	3.01	1.04	0.52	5.13	2.94	2.67	2.04	3.81	2.57	2.26
La	43.8	36.0	33.9	25.3	27.8	31.2	33.0	35.3	32.0	30.9	51.2	56.5	57.6	16.0	41.1	11.9	58.6
Ce	77.6	65.8	60.5	43.7	48.9	56.6	59.1	65.7	65.8	60.3	98.4	119	122	35.4	80.6	25.9	99.2
Pr	9.07	7.97	6.92	5.09	5.58	6.80	6.98	7.85	8.51	7.65	11.9	14.3	13.3	4.88	9.56	3.50	12.5
Nd	33.9	30.3	25.6	18.6	20.3	25.6	26.0	29.8	35.1	30.6	43.6	53.3	48.6	18.0	35.0	13.7	43.9
Sm	5.75	5.43	4.38	3.13	3.16	4.76	4.70	5.48	6.33	5.23	7.63	9.53	8.16	3.52	5.89	2.87	6.78
Eu	1.88	1.83	1.59	0.84	1.13	1.20	1.06	1.27	1.89	1.56	1.73	2.33	1.73	0.80	1.38	0.97	1.18
Gd	4.93	4.70	4.02	2.56	2.91	4.46	4.37	5.14	5.32	4.26	6.58	8.06	6.88	2.96	4.87	2.41	5.31
Tb	0.67	0.69	0.59	0.36	0.37	0.68	0.67	0.79	0.73	0.57	0.87	1.18	0.96	0.46	0.69	0.42	0.73
Dy	3.58	3.69	3.23	1.89	2.09	4.02	3.86	4.56	3.74	2.81	4.34	6.25	5.05	2.46	3.34	2.54	3.70
Ho	0.69	0.73	0.66	0.40	0.46	0.85	0.83	0.96	0.72	0.52	0.79	1.19	0.95	0.46	0.63	0.56	0.67
Er	1.87	2.02	1.87	1.17	1.53	2.33	2.26	2.60	1.83	1.41	1.98	3.14	2.58	1.19	1.65	1.75	1.86
Tm	0.28	0.29	0.29	0.18	0.27	0.35	0.35	0.39	0.25	0.20	0.28	0.45	0.37	0.17	0.24	0.30	0.28
Yb	1.83	1.92	1.94	1.24	2.01	2.31	2.31	2.61	1.61	1.23	1.78	2.94	2.36	1.09	1.53	2.14	1.86
Lu	0.28	0.28	0.31	0.19	0.34	0.34	0.36	0.42	0.24	0.19	0.26	0.44	0.36	0.16	0.23	0.34	0.28
$(La/Yb)_N$	17	13	13	15	10	10	10	10	14	18	21	14	18	11	19	4	23
$(Gd/Yb)_N$	2.2	2.0	1.7	1.7	1.2	1.6	1.6	1.6	2.7	2.9	3.1	2.3	2.4	2.3	2.6	0.9	2.4
Eu/Eu*	1.08	1.12	1.17	0.91	1.14	0.80	0.72	0.74	1.00	1.01	0.75	0.82	0.71	0.76	0.79	1.13	0.61
∑REE	186	161	145	104	117	141	145	162	164	147	231	278	271	87	186	69	236

Note: $CIA = [Al_2O_3/(Al_2O_3 + CaO^* + Na_2O + K_2O)] \times 100$ and $PIA = [(Al_2O_3 - K_2O)/(Al_2O_3 + CaO^* + Na_2O - K_2O)] \times 100$, where CaO^* represents Ca in silicate-bearing minerals only and all in molecular proportions; $ICV = (Fe_2O_3 + K_2O + Na_2O + CaO + MgO + TiO_2)/Al_2O_3$; PAAS from Taylor and McLennan (1985).

tape, then enclosed in epoxy resin and polished to about half their thickness. In order to observe the internal structure of the polished zircons, cathodoluminescence (CL) imaging was carried out using a JXA-8100 Electron Probe Microanalyzer with a Mono CL3 Cathodoluminescence System in the Guangzhou Institute of Geochemistry.

3.2.1. Zircon U–Pb dating

Zircon U–Pb isotope analysis was conducted by a Nu Plasma HR MC-ICP-MS (Nu Instruments, UK) equipped with a 193 nm excimer laser ablation system (Resolution M-50, Resonetics LLC, USA), installed in the Department of Earth Sciences, the University of Hong Kong. Most analyses were carried out using a spot diameter of 30 μm with a repetition rate of 6 Hz. Typical ablation time was about 40 s for every measurement which resulting in pits 30–40 μm depth. The ablated sample aerosol was transported in helium mixed with a small volume of argon and nitrogen to the MC-ICPMS torch for analysis. Masses 232, 208–204 were simultaneously measured in static-collection mode. Standard zircons 91500 and GJ were used as external standards and were analyzed twice before and after every 10 analyses to eliminate the influence of instrumental mass bias, depth-dependent elemental and topic fractionation, while the standard silicate glass NIST 610 was used to optimize the instrument. The detailed analytical technique is described by Xia et al. (2011). The common-Pb correction was carried out using the Excel program ComPbCorr#3 (Andersen, 2002). The dating results are listed in Appendix Table A1.

3.2.2. Lu–Hf isotope analyses

Zircon Lu–Hf isotope analyses were performed using a Nu Plasma HR MC-ICP-MS (Nu Instruments, UK), coupled to a 193 nm excimer laser ablation system (RESOlution M-50, Resonetics LLC, USA), installed in the Department of Earth Sciences, University of Hong Kong. Hf isotopic data were acquired using a 55 μm beam diameter and a 6 Hz repetition rate. Each analytical spot was subjected to 20 ablation cycles, resulting in pits 30–40 μm deep. Atomic masses 172–179 were simultaneously measured in static-collection mode. The measured isotopic ratios of $^{176}Hf/^{177}Hf$ were normalized to $^{179}Hf/^{177}Hf = 0.7325$, using an exponential correction for mass bias. The in situ measured $^{173}Yb/^{172}Yb$ ratio was used for mass bias correction for both Yb and Lu because of their similar physicochemical properties. Ratios used for the corrections were 0.5886 for $^{176}Yb/^{172}Yb$ (Chu et al., 2002) and 0.02655 for $^{176}Lu/^{175}Lu$ (Machado and Simonetti, 2001). External corrections were applied to all unknowns, and standard zircons 91500 and GJ were used as external standards and were analyzed twice before and after every 10 analyses. The measured $^{176}Lu/^{177}Hf$ ratios and the ^{176}Lu decay constant of 1.867×10^{-11} a^{-1} reported by Söderlund et al. (2004) were used to calculate initial $^{176}Hf/^{177}Hf$ ratios. Chondritic values of $^{176}Hf/^{177}Hf = 0.0336$ and $^{176}Lu/^{177}Hf = 0.282785$ reported by Bouvier et al. (2008) were used for the calculation of $\varepsilon_{Hf}(t)$ values. The depleted mantle line is defined by present-day $^{176}Hf/^{177}Hf = 0.28325$ and $^{176}Lu/^{177}Hf = 0.0384$ (Griffin et al., 2004). Two-stage "crustal" model ages (T_{DM}^c) was calculated using a mean $^{176}Lu/^{177}Hf$ ratio of 0.015 for the average continental crust (Griffin et al., 2002). The Lu–Hf isotopic data are listed in Appendix Table A2.

4. Results

4.1. Geochemistry

4.1.1. Major elements

The schists of the Tuoge supracrustal rocks have moderate SiO_2 contents (60.83–69.48 wt%), with large variations in Al_2O_3 (11.24–18.06 wt.%), CaO (1.55–5.19 wt%), Na_2O (0.12–4.34 wt%), and $Fe_2O_3^T$ (2.31–5.80 wt%). In contrast, the slates have higher SiO_2 (71.62–82.47 wt%) and Na_2O (0.89–4.58 wt%), but lower CaO (0.16–2.40 wt%), Al_2O_3 (8.44–15.16 wt%), and $Fe_2O_3^T$

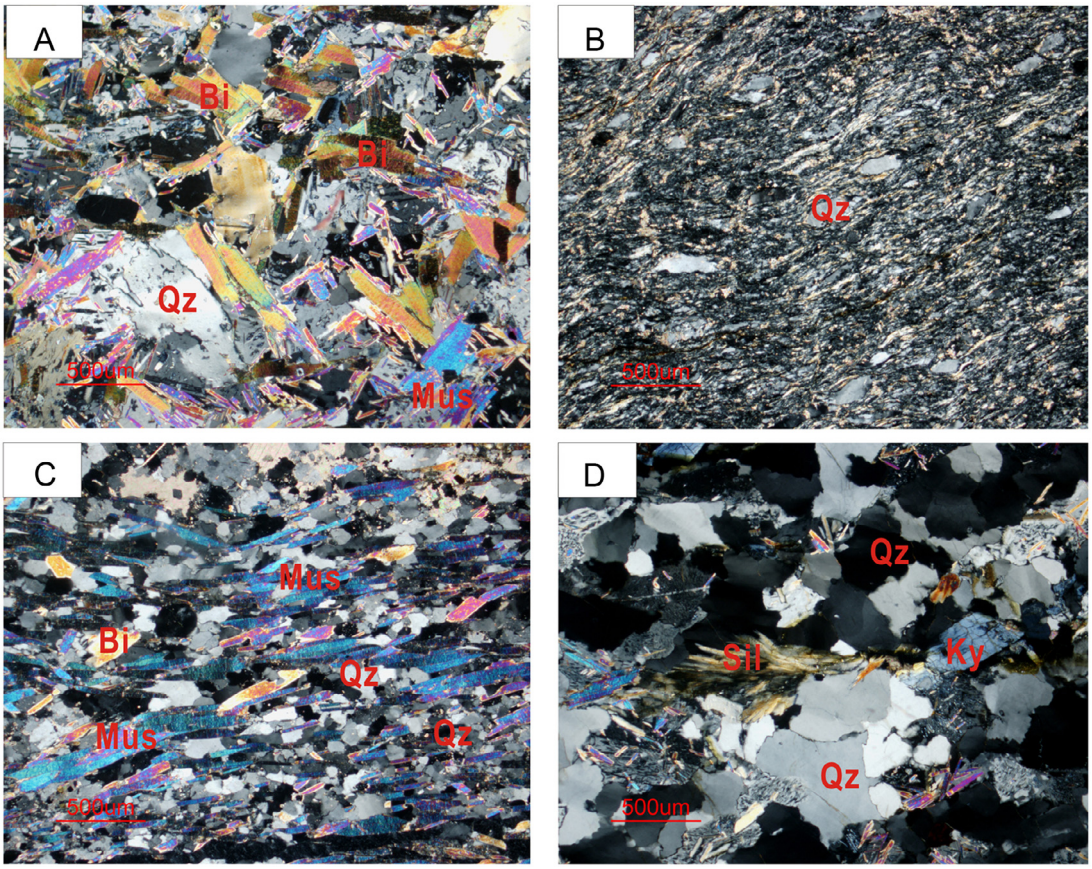

Fig. 3. Textural characteristics of the Paleoproterozoic metasedimentary rocks exposed in the Kuluketage Block. (a) two mica schist of the Tuoge supracrustal rocks; (b) fine-grained slate of the Tuoge supracrustal rocks; (c) muscovite schist of the Xingditage Group; (d) kyanite and sillimanite-bearing mica schist. Under cross-polarized light. (a) and (c) Granoblastic to lepido blastic texture with biotite and muscovite defining the schistosity. The abbreviations for minerals: Qz, quartz; Bi, biotite; Mus, muscovite; Ky, kyanite; Sil, sillimanite.

(0.63–4.12 wt%). Compared to the post-Archean Australian average shale (PAAS) (Taylor and McLennan, 1985), the schists display slightly higher SiO_2, CaO and Na_2O, but lower Al_2O_3 and $Fe_2O_3^T$, whereas the slates have much higher SiO_2, slightly higher CaO and Na_2O, but lower Al_2O_3 and $Fe_2O_3^T$.

Except for sample NT26-4 (SiO_2 = 76.63 wt%), the schists of the Xingditage Group have a relatively narrow range in SiO_2 (52.86–67.76 wt%) contents and show large variations in TiO_2 (0.29–1.16 wt% wt.%), Al_2O_3 (10.12–18.28 wt% wt.%), MgO (0.99–9.04 wt%), CaO (0.80–7.52 wt%), Na_2O (0.33–4.33 wt%) and K_2O (0.49–6.67 wt%). Different from PAAS (Taylor and McLennan, 1985), most of the Xingditage samples display much higher MgO, CaO and Na_2O, but slightly lower SiO_2 and Al_2O_3 (Table 1).

4.1.2. Trace elements

The Tuoge supracrustal rocks show variable rare earth element (REE) patterns in the chondrite-normalized diagram (Fig. 4a). The schists are LREE-enriched and show relatively flat HREE patterns (La_N/Yb_N = 8–63, Gd_N/Yb_N = 1.3–4.9). Compared to PAAS, these rocks have lower ferromagnesian (e.g. Cr, Co and Ni), slightly lower high field-strength elements (HFSE, e.g. Zr, Hf, Nb, Ta and Y) but higher large ion lithophile elements (LILE, e.g. Rb, Ba and Pb, except for Th and U) (Fig. 4b). The slates show moderately LREE-enriched patterns, with relatively flat HREE (La_N/Yb_N = 4–31, Gd_N/Yb_N = 0.9–3.6). Compared to PAAS, the slate samples have slightly lower ferromagnesian and HFSE contents, and slightly higher LILE, with exception of Th and U (Table 1).

The schists of the Xingditage Group display uniform REE patterns in the chondrite-normalized diagram (Fig. 4c), with a narrow range of total REE contents between 87 ppm and 278 ppm (Table 1). Most of the samples are characterized by moderate enrichment in LREE and show relatively flat HREE patterns (La_N/Yb_N = 4–23, Gd_N/Yb_N = 0.9–3.1), similar to that of PAAS (0.63, Taylor and McLennan, 1985). The rocks have weak negative to positive Eu anomalies (Eu/Eu^* = 0.61–1.17), more pronounced than PAAS (0.63, Taylor and McLennan, 1985). For the trace elements, the samples collected from the central Kuluketage Block (near Xinger) and the southern (along the Xingdi River) show different geochemical features (Table 1). The schist samples from the central part are mostly characterized by low ferromagnesian contents, lower LILE and HFSE concentrations than PAAS, with the exception of few samples that have high Sr and Ba contents (Fig. 4d). In contrast, the schist samples from the southern part have higher ferromagnesian and LILE contents than PAAS, but similar HFSE concentrations.

4.2. Zircon U–Pb ages and Hf isotopic compositions

4.2.1. The Tuoge supracrustal rocks

Slate sample Nt03 was selected from for detrital zircon dating (Appendix Table A1). The zircons are transparent, mostly rounded or subrounded, and have lengths between 80 μm and 100 μm. These grains are characterized by very low luminescence, but the development of oscillatory zoning and their high Th/U ratios suggest that most of them are igneous (Th/U > 0.1, weak oscillatory zoning) and only a few grains may have a metamorphic origin (Th/U <0.1, no oscillatory zoning) (Hoskin and Schaltegger, 2003).

In the slate sample (Nt03), the dominant igneous zircon population yields Paleoproterozoic $^{207}Pb/^{206}Pb$ ages ranging from 1.72 Ga

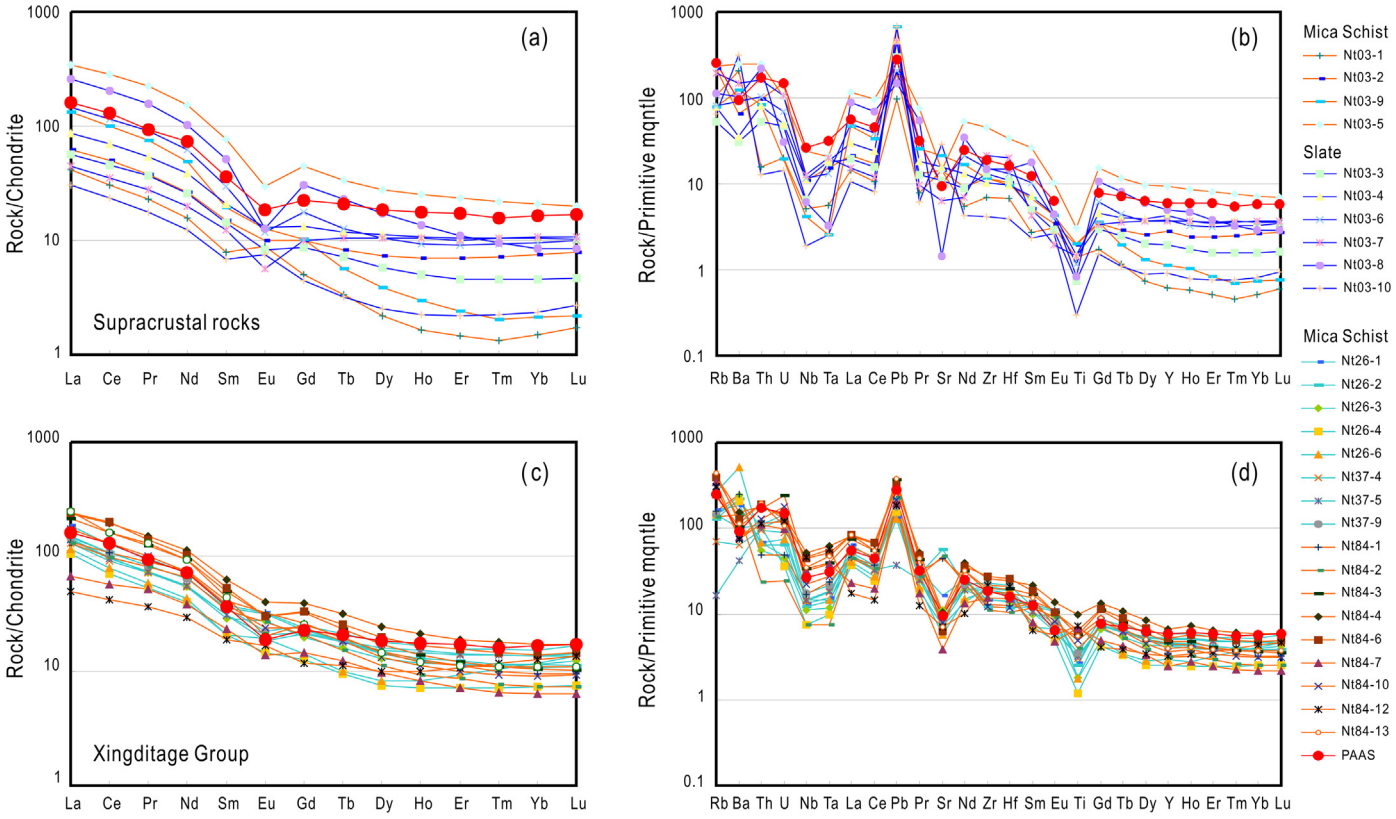

Fig. 4. Chondrite-normalized REE patterns and Upper Crust-normalized spider diagrams for the Paleoproterozoic metasedimentary rocks exposed in the Kuluketage Block. Chondrite and primitive mantle normalizing values are from Sun and McDonough (1989) and PAAS data are from Taylor and McLennan (1985).

to 2.08 Ga (Fig. 5a). Two igneous grains yield early Paleoproterozoic $^{207}Pb/^{206}Pb$ ages of ~2.2 Ga, whereas four grains give older Paleoproterozoic $^{207}Pb/^{206}Pb$ ages of ~2.32 Ga. The unzoned grains from this sample yield late Paleoproterozoic $^{207}Pb/^{206}Pb$ ages between 1.61 Ga and 1.76 Ga. The same zircon grains were analyzed for Hf isotopic compositions (Appendix Table A2). Except for two grains with positive $\varepsilon_{Hf}(t)$ values (+4 and +6), the igneous zircons have large variations in $\varepsilon_{Hf}(t)$ values (−17 to −3) (Fig. 6a), with old Neoarchean crustal model ages (T_{DM}^{c} = 2.6–3.7 Ga). The late Paleoproterozoic unzoned grains yield evolved Hf isotopic compositions, with $\varepsilon_{Hf}(t)$ values ranging from −11 to −3 and T_{DM}^{c} model ages of 2.7–3.0 Ga.

4.2.2. Xingditage Group

Schist sample Nt26 and quartzite sample Nt31 were selected from the upper Xingditage Group, together with schist sample Nt35 from the lower Xingditage Group, for zircon dating (Appendix Table A1). Zircons from the upper Xingditage Group are transparent, subrounded to rounded, and small in size (length: 70–120 μm). Most of the zircons show low luminescence and weak oscillatory zoning with high Th/U ratios (>0.2), indicating an igneous origin. Zircons from the lower Xingditage Group (Nt35) are different. They are dominantly euhedral prismatic or, to a lesser degree, subrounded, and large in size (length: 110–210 μm). They are characterized by low luminescence and distinct oscillatory zoning with high Th/U ratios (mostly >0.5), also suggesting an igneous origin. A few grains from sample Nt31 and Nt35 are highly luminescent, but with low Th/U ratios (<0.1), similar to features of typical metamorphic zircons (Hoskin and Schaltegger, 2003).

In sample Nt26, most zircons mostly give Paleoproterozoic $^{207}Pb/^{206}Pb$ ages between 1.8 Ga and 2.1 Ga, with one discordant grain with $^{207}Pb/^{206}Pb$ age of 2.46 Ga (Fig. 5b). The igneous grains mostly have negative $\varepsilon_{Hf}(t)$ values (−12 to −1) (Fig. 6b) and Paleoproterozoic to Mesoarchean crustal model ages (T_{DM}^{c} = 2.7–3.1 Ga). However, five of the older grains show positive $\varepsilon_{Hf}(t)$ values from +1 to +6 (Appendix Table A2).

Most of the zircons from sample Nt31 yield Paleoproterozoic $^{207}Pb/^{206}Pb$ ages ranging from 1.8 Ga to 2.1 Ga, and are similar to the igneous zircons from sample Nt26. Two zircons give older Paleoproterozoic $^{207}Pb/^{206}Pb$ ages at 2.12 and 2.42 Ga (Fig. 5c). A single zircon recorded an Archean $^{207}Pb/^{206}Pb$ age of 2.50 Ga. With the exception of one grain having a positive $\varepsilon_{Hf}(t)$ value (+9), all other zircons give negative $\varepsilon_{Hf}(t)$ values (−14 to −2) (Fig. 6c) and Archean T_{DM}^{c} ages mostly between 2.7 and 3.1 Ga. A metamorphic grain yields the youngest Paleoproterozoic $^{207}Pb/^{206}Pb$ age of 1.77 Ga, with a low negative $\varepsilon_{Hf}(t)$ value (−12) and old T_{DM}^{c} age at 3.25 Ga.

In sample Nt35, the majority of zircons yield Neoarchean $^{207}Pb/^{206}Pb$ ages (2.5–2.7 Ga), with the exception of three grains having Paleoproterozoic $^{207}Pb/^{206}Pb$ ages of 1.94, 2.09 and 2.31–2.49 Ga (Fig. 5d). Except for one grain with a positive $\varepsilon_{Hf}(t)$ value (+1), the others give negative $\varepsilon_{Hf}(t)$ values between −7 and −1 (Fig. 6d) with Archean crustal model ages (T_{DM}^{c} = 3.14–3.51 Ga). Three metamorphic grains yield similar Paleoproterozoic $^{207}Pb/^{206}Pb$ ages of ~2.22 Ga, with one of slightly negative $\varepsilon_{Hf}(t)$ value (−1) and T_{DM}^{c} age of 3.21 Ga and two having more negative $\varepsilon_{Hf}(t)$ values (−10) and older T_{DM}^{c} ages (~3.45 Ga).

5. Discussion

5.1. Depositional age

5.1.1. The supracrustal rocks within the Archean TTG

The supracrustal rocks within the Archean TTGs and the TTGs exposed in the Kuluketage Block were both previously considered

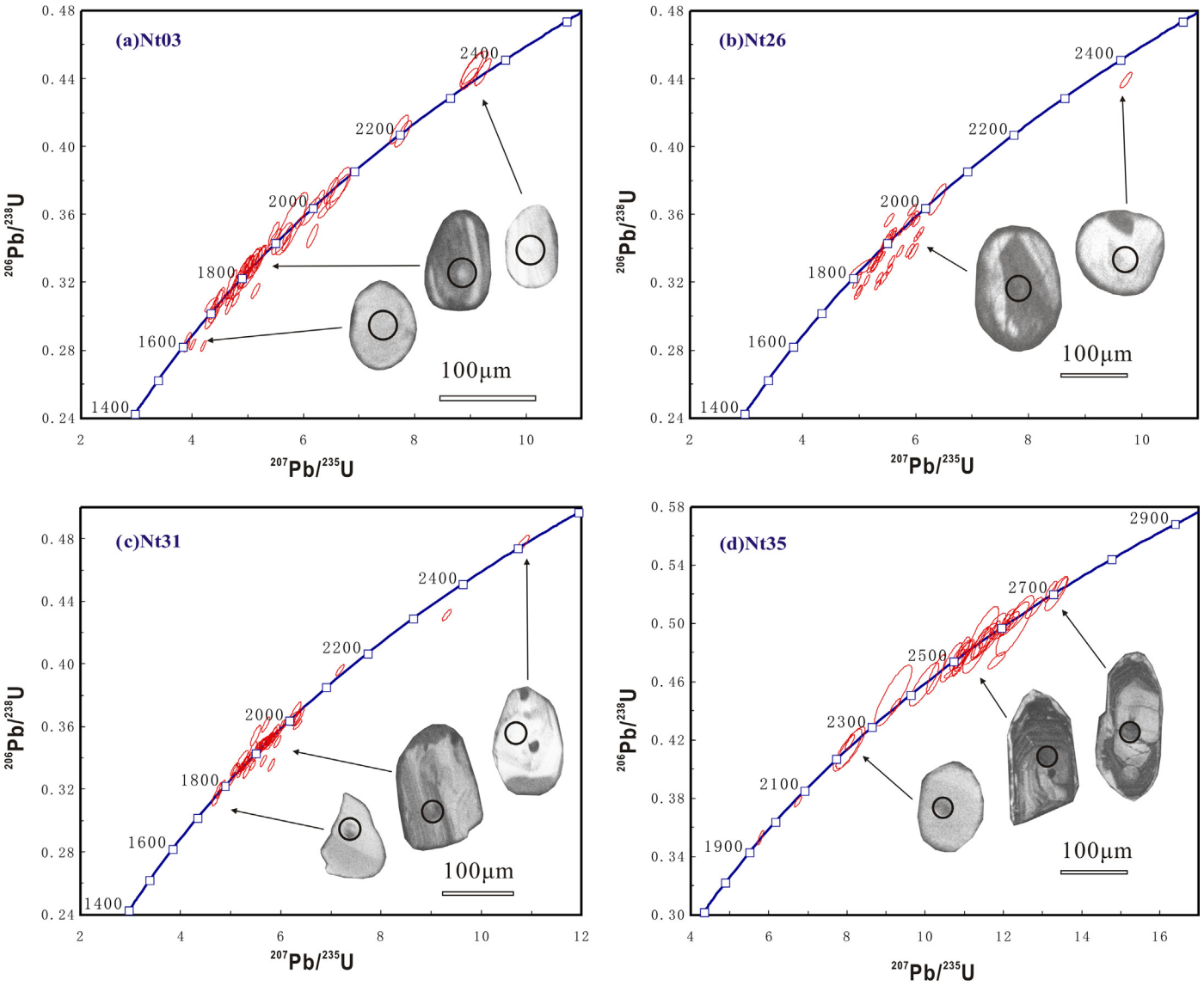

Fig. 5. Zircon U–Pb concordia diagrams for the Paleoproterozoic metasedimentary rocks. The circles on zircons show the locations of U–Pb dating. (a) Slate sample from the Tuoge supracrustal rocks; (b) schist from the upper Xingditage Group; (c) quartzite from the upper Xingditage Group; (d) schist from the lower Xingditage Group.

to be the oldest basement rocks of the northern Tarim Craton, originally named as the Tuogelakebulake Group (RGS, 1965) but later referred to as the Dagelakebulake Group (XBGMR, 1993; GCRSX, 1981). Then they were named the Tuoge Complex (Hu and Rogers, 1992; Hu et al., 1997, 2000). Because of the proposed Neoarchean depositional age for the overlying Xinditage Group and the angular unconformity at the base of this group, the Tuoge Complex including the metamorphic supracrustal rocks was originally assigned a Paleoarchean age (RGS, 1965). In the early 1990s, amphibolites from the supracrustal rocks were dated for the first time using the whole-rock Sm–Nd isochron method (Hu and Rogers, 1992). On the basis of the Sm–Nd isochron age (3263 ± 129 Ma), these authors suggested that the Tuoge supracrustal rocks were deposited in the Paleoarchean and thus they argued a Paleoarchean basement existed in the northern Tarim Craton (Hu and Rogers, 1992). More recently, some Archean Rb–Sr isochron and Nd model ages ranging from 2.8 to 3.4 Ga were also reported for the metamorphic supracrustal rocks (Feng et al., 1995; Hu et al., 1997, 2000). However, because the above age data generally have poor precision, the precise age of these supracrustal rocks were still poorly constrained.

Recently, a systematic Sr–Nd isotopic study on the amphibolites exposed near Korla yielded large variation of Nd model ages between 1545 Ma and 3380 Ma (Guo et al., 2003). Four zircon grains from an amphibolite, however, yielded a late Paleoproterozoic upper intercept age of 1836 ± 25 Ma, whereas four zircon grains from a hornblende-bearing paragneiss gave an early Paleoproterozoic upper intercept age of 2492 ± 19 Ma (Guo et al., 2003). In this study, the U–Pb ages of detrital zircons from the Tuoge supracrustal rocks reveal a predominant igneous population formed in the middle Paleoproterozoic between 1.76 Ga and 2.08 Ga (Fig. 7a). The youngest zircon population in this sample yields a late Paleoproterozoic age peak at 1.63 Ga. Although the youngest zircons are unzoned, their subrounded to rounded shapes without wide metamorphic rims and the low-grade metamorphism of their protoliths indicate that these grains were detritus and not formed by post-depositional metamorphism. We suggest that the ages (1.63 Ga) of the youngest zircons define the maximum depositional age of the

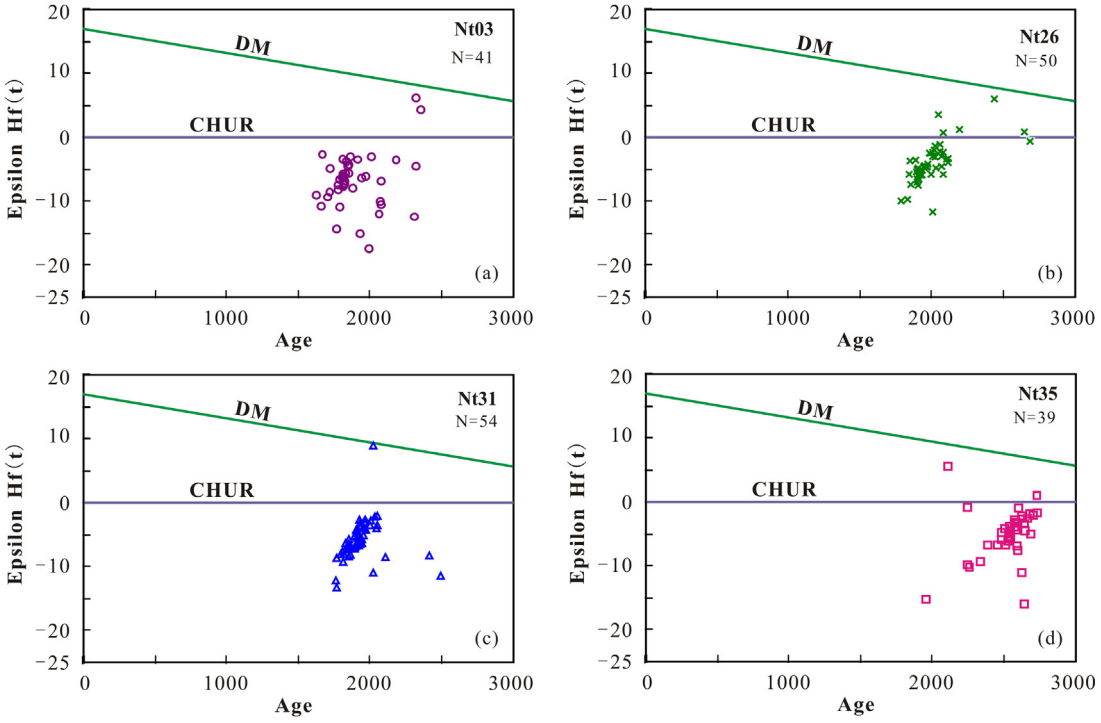

Fig. 6. $\varepsilon_{Hf}(t)$ versus age diagrams for detrital zircons from the Paleoproterozoic metasedimentary rocks.

supracrustal rocks, which is clearly much younger than previously thought. Therefore, the supracrustal rocks exposed in the TTGs were deposited after the late Paleoproterozoic and should not be considered as a part of the Archean basement.

5.1.2. The Xingditage Group

The Xingditage Group was first shown on the early 1:200,000 geological maps and it was suggested to have formed in the Neoarchean, although there was no geochronological evidence (RGS, 1965). In 1981, the group was defined as the oldest cover in the northern Tarim Craton and assigned to the Paleoproterozoic during a detailed stratigraphic investigation of Northwest China (GCRSX, 1981). This formation age was generally accepted and used in later studies, but there were no reliable age data provided (BGMRX, 1993; Hu et al., 1997, 2000).

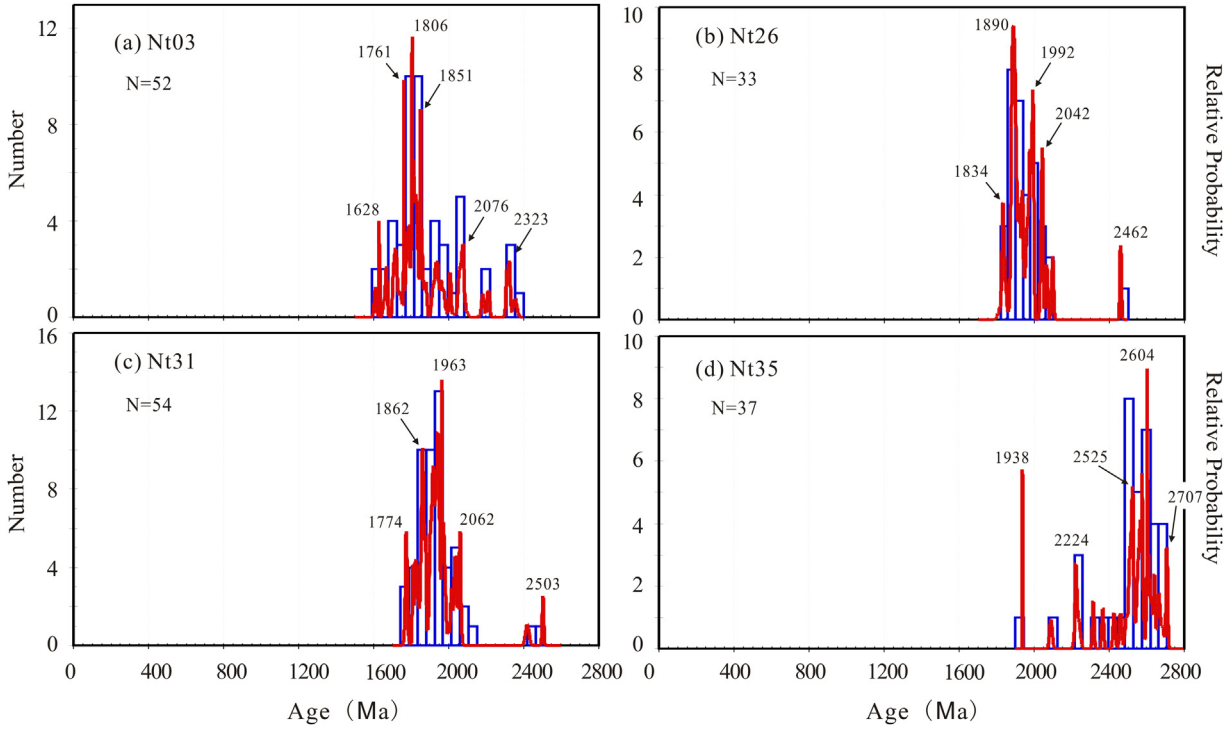

Fig. 7. Relative probability plots for detrital zircons from the Paleoproterozoic metasedimentary rocks.

Recently, five zircon grains from a gneissic granitic pluton to the south of Xinger were dated by the ID-TIMS method and yielded a late Paleoproterozoic upper intercept age of 1836 ± 25 Ma (Guo et al., 2003). Based on the angular unconformity between the granitic pluton and the overlying Xingditage Group, Guo et al. (2003) proposed that the depositional age of the group was not prior to 1.8 Ga. Several years later, a comparative study of C isotopic variation patterns of marbles from the Xingditage Group and the Chuanlinggou and Dahongyu formations of the North China Craton suggested that the Xingditage Group in the Kuluketage Block was most likely deposited in the late Paleoproterozoic (Yang et al., 2010). However, more recent U–Pb dating of detrital zircons from the Xingditage Group suggested that the source materials mainly formed between 2.8 and 2.2 Ga and were metamorphosed at 1.9–1.8 Ga (Zhang et al., 2012a). The metamorphic age is thus considered as defining the maximum depositional age of the Xingditage Group (Zhang et al., 2012a). We note that these studies focus on the high-grade metamorphic rocks collected from the lower Xingditage Group.

In this study, the U–Pb results of the three metasedimentary samples from the Xingditage Group show different age spectra (Fig. 7b-d). The detrital zircons from the schist sample (Nt26) from the upper Xingditage Group are dominated by middle Paleoproterozoic igneous grains (1.76–2.08 Ga) and yield a youngest age peak (1.83 Ga), younger than that presented in a recent study (~2.0 Ga; Ge et al., 2014b). Zircon U–Pb dating of the quartzite sample (Nt31) reveals a dominant igneous population (1.86–2.06 Ga) with ages similar to those from sample Nt26. Two youngest zircons from the quartzite formed at 1.77 Ga, including one igneous and one metamorphic grain. The rounded shape of this metamorphic grain indicates long transportation and thus suggests that it was not formed in post-depositional metamorphism. In contrast, the other schist sample (Nt35) from the lower Xingditage Group has igneous detrital zircons mostly formed in the Neoarchean (2.5–2.7 Ga). In this sample, two igneous zircons yield the youngest Paleoproterozoic ages at 1.94 and 2.09 Ga. On the basis of the youngest detrital zircons, we suggest that the youngest ages at 1.77 Ga and 1.94 Ga defines the maximum depositional ages for the upper and the lower Xingditage Group, respectively.

Because the Tuoge supracrustal rocks share a large amount of ~1.75–2.05 Ga source materials with the upper Xingditage Group and have similar depositional ages, we suggest that the supracrustal rocks in the Archean TTGs are parts of the upper Xingditage Group. The supracrustal lenses in the Tuoge Complex were thus most likely the result of intense regional post-depositional deformation which has led to their tectonic interleaving with the Archean TTGs.

5.2. Source characteristics

Whole-rock geochemical features are able to trace the weathering characteristics and source composition of sedimentary rocks (McLennan et al., 1993; Bhat and Ghosh, 2001). There are some commonly used parameters, such as the Chemical Index of Alteration (CIA), the Plagioclase Index of Alteration (PIA) and the Index of Compositional Variability (ICV) (Cox et al., 1995; Fedo et al., 1995; Cullers and Podkovyrov, 2000). The schists of the Tuoge supracrustal rocks have low CIA values between 45 and 56, whereas the slate samples show CIA values of 49–63 (Fig. 8a). These values indicate that the schist and slate are not strongly weathered, or that compositionally mature alumina-rich minerals were absent in the source (Nesbitt and Young, 1982; Fedo et al., 1995). Although the Xingditage schists have large variations of CIA values (37–67), their generally lower CIA values than that of PAAS (69) suggest that they were also derived from a weakly weathered source. This conclusion is also supported by their respective PIA values (mostly 43–57 for the schists and slates of Tuoge supracrustal rocks, and mostly 37–60 for the Xingditage schists), because fresh felsic rocks have PIA values of 50 and the PIA values of clay minerals such as kaolinite, illite and gibbsite are close to 100 (Fedo et al., 1995). Sediments with low ICV values may have been derived from mature sediments with a high percentage of clay minerals, whereas sediments with high ICV may represent first cycle deposits (Kamp and Leake, 1985). The schist samples from both the Xingditage Group and the Tuoge supracrustal rocks have ICV values mostly between 1.0 and 2.0 (Table 1), which suggests that the metasediments were derived from a source compositionally dominated by immature material and poor in alumina-rich minerals (Fedo et al., 1995). The slate samples, however, show relatively low ICV values (0.67–1.21), indicative of a somewhat more mature material source.

In the ACNK (ACNK = molar ratio of $Al_2O_3/[CaO + Na_2O + K_2O]$) diagram (Fig. 8b), the schists and slates of the Tuoge supracrustal rocks plot near the average tonalite and granodiorite line, which implies fresh feldspars in the source and that the source materials did not experience significant chemical weathering (Nesbitt and Young, 1984; Fedo et al., 1995). However, the Xingditage schists plot away from the predicted weathering trend of tonalite-granodiorite-granite in the ACNK diagram, which suggests that these metasediments were probably altered by post-depositional K-metasomatism.

The Th/Sc ratios can be used to trace the sedimentary provenance, because Th is enriched in silicic rocks relative to basic rocks and Sc is more enriched in basic than silicic rocks, and the ratio does not vary significantly during sedimentary recycling (Cullers, 1994). In contrast, the Zr/Sc ratios will increase considerably during sediment recycling, and thus it can be considered as a useful indicator of zircon enrichment (McLennan, 1989). The schists and slates of the Tuoge supracrustal rocks give the highest Th/Sc (0.74–7.16, with one exception of 0.32) and Zr/Sc ratios (11.48–65.78) (Table 1). The Xingditage schists, however, show relatively narrow variations in Th/Sc (0.08–0.77) and Zr/Sc ratios (4.96–24.62). Although these rocks have different Th/Sc and Zr/Sc ratios, they define a strong positive correlation in the Th/Sc–Zr/Sc diagram (Fig. 9a), which indicates that geochemical variation was dominated by the composition of the source materials and not sediment recycling (Cullers, 1994).

The La/Th ratios and Hf contents are also sensitive indices of the source composition of clastic rocks (Floyd and Leveridge, 1987). In the La/Th–Hf diagram (Fig. 9b), the metasediments of both the Xingditage Group and the Tuoge supracrustal rocks plot in the acidic arc or andesitic arc fields, indicating that the source materials were dominated by felsic igneous rocks from a magmatic arc. This conclusion is also supported by the major population of igneous detrital zircons formed in a short time span between 1.76 Ga and 2.08 Ga (Fig. 7a–d).

5.3. Tectonic setting

The Paleoproterozoic was a pivotal time for the evolution of continental crust and is characterized by worldwide collisional orogens formed at ~1.8 Ga (Condie, 2002; Rogers and Santosh, 2002; Wilde et al., 2002; Zhao et al., 2002, 2004). In the Tarim Craton, the Paleoproterozoic Xingditage Group and Mesoproterozoic Yangjibulake Group were generally suggested to have been deposited along a passive continental margin because of their thick mature sediments and carbonates (GCRSX, 1981; BGMRX, 1993). The passive margin tectonic setting appears to be supported by the early Paleoproterozoic rift-related intrusive rocks exposed in the southwestern Tarim Craton, including mafic dykes, A-type granites as well as possible volcanic rocks, which were suggested to have been produced in an extensional environment based on their whole-rock geochemistry (Zhang et al., 2007a; Lu et al., 2008). However, the geochemistry

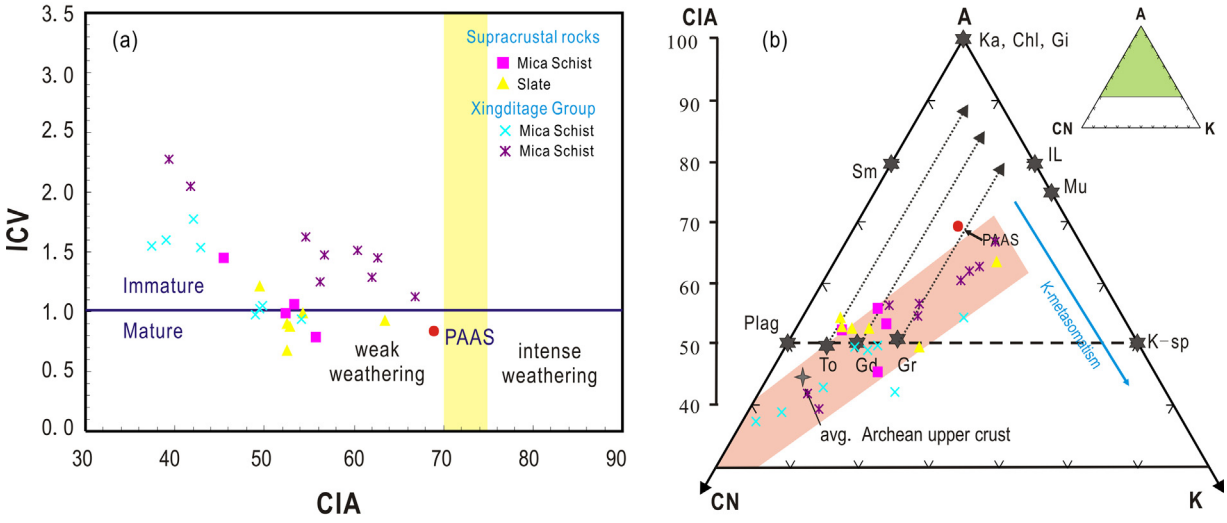

Fig. 8. (a) CIA–ICV diagram for the Paleoproterozoic metasedimentary rocks of the Kuluketage Block (after Nesbitt and Young, 1984; Cox et al., 1995). (b) ACNK diagram for the Paleoproterozoic metasedimentary rocks (after Nesbitt and Young, 1984; Fedo et al., 1995). Data for tonalite (To), granodiorite (Gd), granite (Gr) and average Archean upper crust are from Condie (1993). PAAS is post-Archean Australian average shale (Taylor and McLennan, 1985). Arrows show the predicted weathering trends of To, Gd and Gr. The abbreviations for minerals: Pl, plagioclase; K-sp, potassic feldspar; Ka, kaolinite; Chl, chlorite; Gi, gibbsite; Sm, smectite; Il, illite; Mu, muscovite; An, anorthite; By, bytownite; La, labradorite; Ad, andesine; Og, oligoclase; Ab, albite.

of the metasediments from the Xingditage Group is not consistent with this interpretation.

It is well established that different tectonic settings can be constrained by the whole-rock geochemistry of sedimentary rocks (Bhatia and Taylor, 1981; Roser and Korsch, 1986; McLennan et al., 1990). For sediments deposited in four typical tectonic settings, i.e. oceanic island arc, continental arc, active continental margins and passive continental margins, Al_2O_3, $Fe_2O_3{}^T + MgO$ and TiO_2 and Al_2O_3/SiO_2 ratios generally decrease in sandstones from oceanic island arc to passive margins, whereas SiO_2 increase (Bhatia, 1983; Bhatia and Crook, 1986). The schists of the Tuoge supracrustal rocks have moderate SiO_2 (mean = 65.58 wt.%), TiO_2 (mean = 0.51 wt.%), Al_2O_3 (mean = 15.08 wt.%), CaO (mean = 3.31 wt.%), MgO (mean = 2.04 wt.%), $Fe_2O_3{}^T + MgO$ (mean = 6.02 wt.%), and relatively high Al_2O_3/SiO_2 (mean = 0.23) ratios, which are distinct from the graywackes in oceanic island arcs and passive margins (Table 2), but share a geochemical affinity with the graywackes from continental arcs. The Xingditage schists show similar chemical compositions to the schists of the Tuoge supracrustal rocks with higher $Fe_2O_3{}^T + MgO$ (mean = 9.96 wt.%) and slightly lower SiO_2 (mean = 61.21 wt.%), also indicating a continental island arc setting. The slates of the Tuoge supracrustal rocks, however, have high SiO_2 (mean = 77.23 wt.%), low TiO_2 (mean = 0.25 wt.%), Al_2O_3 (mean = 11.18 wt.%), CaO (mean = 1.66 wt.%), MgO (mean = 1.21 wt.%), $Fe_2O_3{}^T + MgO$ (mean = 3.45 wt.%), and relatively low Al_2O_3/SiO_2 (mean = 0.14) ratios, similar to those of graywackes from active continental margins (Table 2). This conclusion is also supported by the trace element compositions of the metasediments which mostly show strong similarities to graywackes from continental arcs (Table 2). In the La–Th–Sc and Th–Sc–Zr/10 triangle diagrams (Bhatia and Crook, 1986), most of the Xingditage schists and the Tuoge supracrustal rocks plot in the continental arc field (Fig. 10). In combination with the weak weathering characteristics and immature source composition, we suggest that the Xingditage schists and the Tuoge supracrustal rocks were deposited in a basin adjacent to a continental arc. Therefore, the Kuluketage Block was most likely in an active continental margin setting during the late Paleoproterozoic.

It is well accepted that the Tarim Craton have recorded the assembly of the Columbia supercontinent, but its location in the supercontinent is poorly constrained (Zhao and Cawood, 2012; Shu et al., 2011; Long et al., 2012a; Xu et al., 2013; Zhang et al., 2013a, 2013b; Ge et al., 2013). Following the assembly of this supercontinent at ~1.8 Ga, it developed both passive and active margins (Rogers and Santosh, 2002; Zhao et al., 2004). The passive continental margins were characterized by large-scale extension, as recorded 1.80–1.75 Ga continental rifting and anorogenic magmatism developed in the Yangtze Craton and other blocks of the

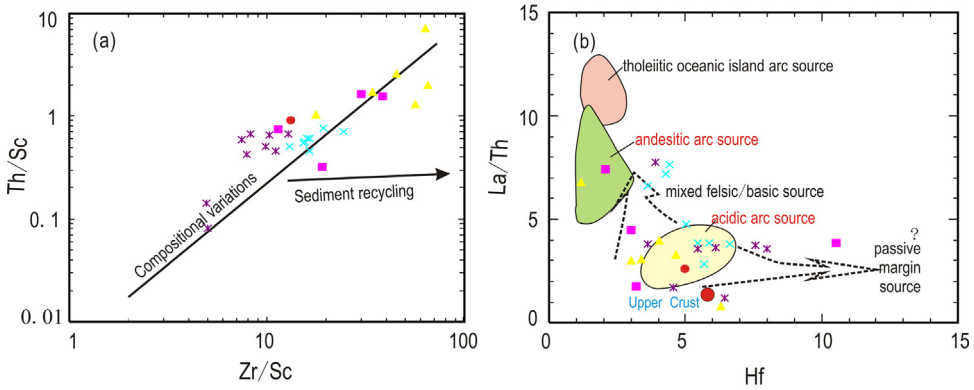

Fig. 9. Geochemical diagrams showing variations of weathering and source composition for the Paleoproterozoic metasedimentary rocks. (a) Th/Sc–Zr/Sc diagram after McLennan et al. (1993); (b) La/Th–Hf diagram after Floyd and Leveridge (1987). Upper crust data are from Taylor and McLennan (1985). Symbols are same to those in Fig. 8.

Table 2
Average chemical compositions of Paleoproterozoic metasedimentary rocks in the Kuluketage Block and representative clastic rocks from various tectonic settings.

Tectonic setting	OIA	CIA	ACM	PM	The supracrustal schists		The supracrustal slates		The Xingditage schists	
Samples	Greywackes				Range	Average	Range	Average	Range	Average
SiO_2	59	71	74	82	60.83–69.48	65.58	71.62–82.47	77.23	52.86–76.63	61.21
TiO_2	1.06	0.64	0.46	0.49	0.33–0.73	0.51	0.08–0.37	0.25	0.20–1.66	0.84
Al_2O_3	17	14	13	8	11.24–18.06	15.08	8.44–15.16	11.18	6.96–18.28	14.64
CaO	5.8	2.7	2.5	1.9	1.55–5.19	3.13	0.16–2.40	1.66	0.80–7.52	3.68
MgO	3.7	2.0	1.2	1.4	1.29–3.28	2.04	0.91–3.34	1.21	0.99–9.04	3.45
$Fe_2O_3{}^T + MgO$	11.7	6.8	4.3	4.7	3.60–7.87	6.02	0.95–5.41	3.45	4.51–17.00	9.96
$K_2O + Na_2O$	5.5	5.0	5.7	2.8	3.63–7.61	6.02	3.22–7.38	4.85	3.06–8.52	5.87
Al_2O_3/SiO_2	0.3	0.2	0.2	0.1	0.17–0.30	0.23	0.10–0.21	0.14	0.09–0.31	0.24
Ba	370	444	522	253	460–1716	1122	213–2235	850	292–3636	1109
Pb	7	15	24	16	6.98–48.0	22	10.6–47.5	26.7	2.64–26.7	15.1
Th	2	11	19	17	1.33–21.0	9.43	1.08–18.9	8.93	2.04–16.5	9.10
U	1	3	4	3	0.43–3.15	1.54	0.30–2.24	1.11	0.52–5.13	2.13
Zr	96	229	179	298	79–515	213	46.4–238	148	126–308	203
Hf	2.1	6.3	6.8	10.1	2.09–10.5	4.71	1.19–6.30	3.76	3.23–7.97	5.28
Nb	2.0	8.5	10.7	7.9	2.93–17.2	7.9	1.34–9.14	5.99	5.40–36.9	16.6
Nd	11	21	25	29	7.41–72.1	28	5.75–28.9	20.4	13.7–53.3	31.3
La_N/Yb_N	2.8	7.5	8.3	10.8	8–63	29	4–31	14	3.97–22.6	14.0
Eu/Eu^*	1.0	0.8	0.6	0.6	0.51–1.43	0.92	0.33–1.38	0.71	0.61–1.17	0.90
Th/U	2.1	4.6	4.8	5.6	2.6–17.1	6.1	3.5–29.8	8.0	2.8–12	4.3
Zr/Hf	46	36	26	30	38–49	45	36–43	39	37–41	38

Abbreviations: OIA, oceanic island arc; CIA, continental island arc; ACM, active continental margins; PM, passive margins.
$Eu/Eu^* = 2 \times Eu_N/(Sm_N + Gd_N)$.
Data for graywackes deposited in various tectonic settings are from Bhatia (1983, 1985) and Bhatia and Crook (1986); $Fe_2O_3{}^T$ of these graywackes are calculated from Fe_2O_3 and FeO: $Fe_2O_3{}^T = Fe_2O_3 + FeO/0.8991$.

Columbia supercontinent (Rogers and Santosh, 2002; Zhao et al., 2005, 2009; Hou et al., 2008). These active continental margins were marked by long-lived (1.8–1.3 Ga), subduction-related outward accretion, as indicated by 1.8–1.3 Ga magmatic arcs covering the present southern and southeastern margins of Laurentia, the southern margin of Baltica, the northwestern margin of Amazonia, the southern and eastern margins of the North Australia Craton, and the southern margin of the North China Craton (Karlstrom et al., 2001; Zhao et al., 2002; Rogers and Santosh, 2004). These sites are characterized by juvenile volcanic sequences and granitoid suites resembling those of present-day island arcs and active continental margins (Geraldes et al., 2001; Hou et al., 2008; Zhao et al., 2009; He et al., 2009, 2010; Santosh, 2010). In the northern Tarim Craton, 1934–1944 Ma granites were recently discovered near Korla city and these were suggested to have been generated in an arc-related setting because of their continental-arc-type geochemical signatures (Lei et al., 2012). To the east, ~2.0 Ga mafic rocks exposed in the Dunhuang Block are characterized by moderate enrichments in LREE and LILE, and depletions in Nb, Ta, Zr, Hf and Ti, also indicative of an active continental margin setting. Incorporating data on the depositional age and tectonic settings of the Xingditage Group and the Tuoge supracrustal rocks, oceanic subduction beneath the northern Tarim Craton most likely began in the middle Paleoproterozoic and continued until the early Mesoproterozoic. This indicates an outboard position of the Tarim Craton in the Columbia supercontinent, which is in agreement with the reconstruction of Columbia proposed by Zhao et al. (2002), in which the Tarim Craton was located between the South China and Australian blocks on the northwest margin of the supercontinent (Zhao et al., 2002, 2004). The ~1.47 Ga metadiabase sills in the northern Tarim Craton with OIB-like geochemical features were suggested to have been produced by high degree partial melting of enriched continental lithospheric mantle within a continental rifting setting (Wu et al., 2014). This work indicates that southward subduction probably terminated at this time and then the northern Tarim Craton transformed into a passive continental margin.

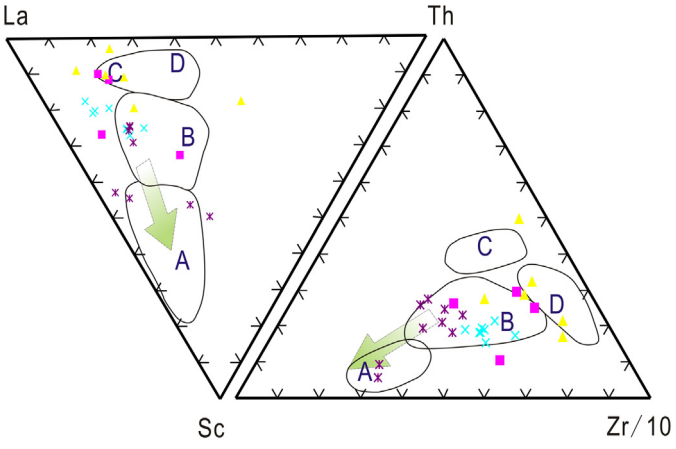

Fig. 10. Tectonic discrimination diagrams for the Paleoproterozoic metasedimentary rocks (after Roser and Korsch, 1986; Bhatia and Crook, 1986). Abbreviations for tectonic settings: A, oceanic island arc; B, continental arc; C, active continental margin; D, passive continental margin. Symbols are same to those in Fig. 8.

5.4. Crustal growth in the northern Tarim Craton

The early Precambrian is a pivotal period for the crustal growth of continent crust (Condie et al., 2011). In the Tarim Craton, early crustal growth history is poorly constrained because of the limited exposure of basement rocks (Hu and Rogers, 1992; Lu et al., 2008). On the basis of a Paleoarchean Sm–Nd isochron age (3263 ± 129 Ma) obtained from amphibolite of the Tuoge Complex, the crustal growth of the northern Tarim Craton was considered to start in the Paleoarchean (Hu and Rogers, 1992). Similar old whole-rock Nd model ages (~3.3 Ga) were also reported for amphibolites exposed at the northern margin of this craton (Guo et al., 2003). In recent Hf isotopic studies of Archean basement rocks (Fig. 11a), zircons from the orthogneisses (2.52–2.65 Ga) in the same region yielded weakly negative $\varepsilon_{Hf}(t)$ values (−5 to +1), but their old two-stage model ages (2.9–3.3 Ga) suggest that the crustal growth started in the Paleoarchean and no crustal materials older than 3.3 Ga existed in the northern Tarim Craton (Long et al., 2010, 2011a). Based on the strongly negative $\varepsilon_{Hf}(t)$ values (mostly between −10 and −28) of Paleoproterozoic detrital zircons from high-grade metamorphic migmatites near Korla city and their oldest $T_{DM}{}^c$ age at 4.32 Ga, Ge et al. (2013) argued that continental crust

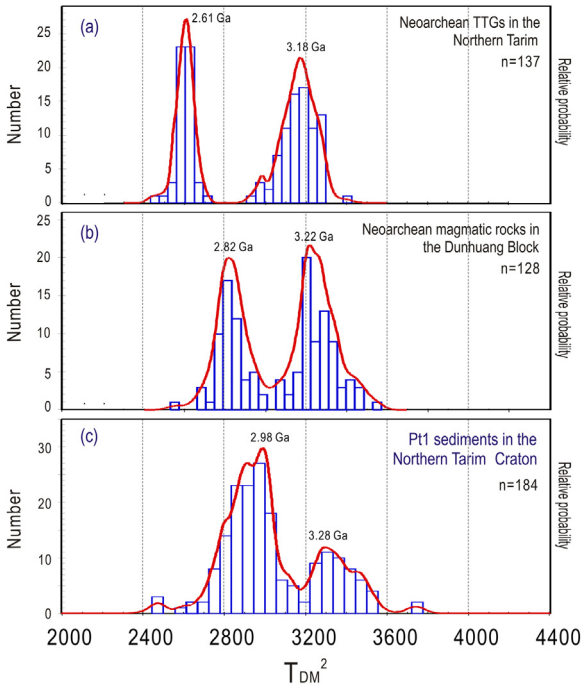

Fig. 11. Relative probability plots for detrital zircons from the Paleoproterozoic metasedimentary rocks compared to those of igneous zircons from the Archean magmatic rocks in the northern Tarim Craton and in the Dunhuang Block, eastern Tarim Craton. (a) Data for the northern Tarim Craton from Long et al. (2010, 2011a). (b) Data for the Dunhuang Block from Zong et al. (2013) and Long et al. (2014). (c) Data for the Paleoproterozoic metasedimentary rocks from this study.

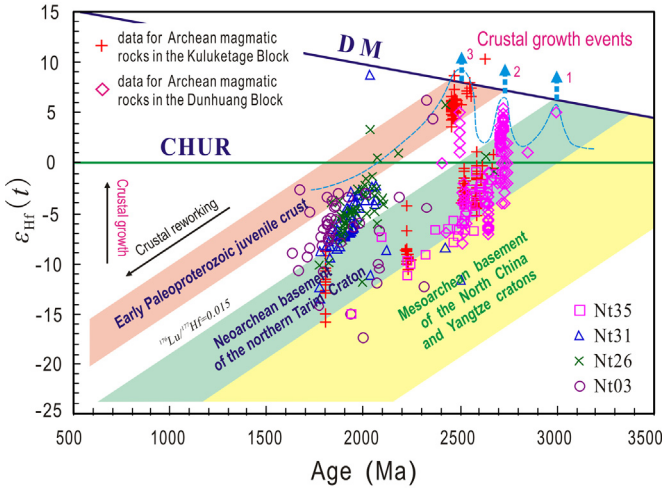

Fig. 12. Hf isotopic compositions of all published detrital zircons from the Paleoproterozoic metasedimentary rocks. Published data for igneous zircons from the Archean basement rocks in the northern Tarim Craton are from Long et al. (2010, 2011a) and those in the Dunhuang Block from Zong et al. (2013) and Long et al. (2014).

older than ca. 3.3 Ga might have existed in the northern Tarim Craton. The two oldest Archean detrital zircons in their study, however, only have T_{DM}^c model ages of 2.48 Ga and 3.37 Ga (Ge et al., 2013). We note that younger garnet-bearing leucosome veins intruded the migmatites and different $^{176}Lu/^{177}Hf$ ratios (lower crust: 0.0093; average continental crust: 0.015) were used in the above studies to calculate the two-stage Hf model ages of zircons, which may be partially the reason for these contrasting interpretations. In the eastern Tarim Craton, however, the oldest record of continental crust is several zircons from a granitic gneiss of the Aketashitage Complex that record an ID-TIMS upper intercept age of ~3.6 Ga (Li et al., 2001). However, this age is suspect because of the complex structure of these zircons. Our previous zircon Lu–Hf isotopic data for TTG gneisses of the Aketashitage Complex reveal similar T_{DM}^c model ages ranging from 3.1 Ga to 3.5 Ga (Fig. 11b), and thus probably indicates the Paleoarchean crustal growth in the eastern Tarim Craton (Long et al., 2014).

In this study, Hf isotopic analyses of the igneous detrital zircons from the Paleoproterozoic metasedimentary rocks reveal two important populations with two-stage model age peaks at ~3.28 and ~2.98 Ga, respectively (Fig. 11c). The older group, dominated by Paleoarchean ages, is consistent with the crustal model ages of igneous zircons from the oldest TTG rocks exposed in both the northern and the eastern Tarim Craton (Fig. 11a and b), and therefore suggests that the earliest crustal growth events in the whole of the Tarim Craton most likely occurred in the late Paleoarchean. Two igneous zircon grains from the Xingditage Group give Eoarchean two-stage model ages at 3.50 Ga and 3.75 Ga. Similar ages (~3.5 Ga) were recently obtained by U–Pb dating of detrital zircons from Paleoproterozoic metasediments in the northern Tarim Craton (Ge et al., 2014b). Because these zircons are rounded and such age information has not been discovered in the igneous basement rocks, we infer that the two grains were possibly derived from nearby old blocks after the assembly of the Columbia supercontinent, instead of the Tarim Craton itself. The younger group, dominated by Meso- to Neoarchean two-stage model ages with a peak at ~2.98 Ga, has negative $\varepsilon_{Hf}(t)$ values ranging from −14 to −2 (Fig. 12). These values plot between the evolutionary trends of the Neoarchean basement and early Paleoproterozoic juvenile crust, indicating a mixed origin formed by reworking of old crustal materials with significant input of juvenile materials. Because of their negative $\varepsilon_{Hf}(t)$ values and absence of coeval juvenile magmatic rocks, we suggest that the late Mesoarchean age peak (~2.98 Ga) does not define juvenile crustal growth events in the northern Tarim craton. In the eastern Tarim Craton, however, zircons from ~2.71 Ga trondhjemitic gneisses near Dunhuang city and a ~2.50 Ga metadiorite in the northern Altyn Tagh have positive $\varepsilon_{Hf}(t)$ values between +1 and +5, indicating that two crustal growth events with significant input of juvenile materials occurred in the early Neoarchean and at the beginning of the Paleoproterozoic (Long et al., 2014). Similar ~2.50 Ga tonalitic gneisses were also discovered near Dunhuang city, of which the zircons have extremely high $\varepsilon_{Hf}(t)$ values up to +7 (Zhang et al., 2013b). In the northern Tarim Craton, the younger growth event was recorded by some ~2.46 Ga orthogneisses which have dominantly early Paleoproterozoic igneous zircons with strongly positive $\varepsilon_{Hf}(t)$ values between +4 and +10 (Long et al., 2010). There three periods of crustal growth are consistent with a recent statistical study of published Nd isotopic data for the basement rocks the Tarim Craton, in which the Nd model ages vary mainly from 2.34 Ga to 3.3 Ga and show peaks at 2.53 Ga, 2.74 Ga and 3.2 Ga (Zhang et al., 2013a).

Based on the above discussion, we suggest that three important early Precambrian crustal growth events developed in the Tarim Craton with significant input of juvenile materials (Fig. 12). The growth events occurred at the late Paleoarchean, the early Neoarchean and at the beginning of the Paleoproterozoic.

6. Conclusions

(1) The metasediments of the upper and lower Xingditage Group in the northern Tarim Craton were deposited after the Paleoproterozoic (<1.77 and <1.94 Ga, respectively). The Tuoge supracrustal rocks were deposited after the late Paleoproterozoic (<1.63 Ga) and are part of the Xingditage Group instead of part of the Archean basement.

(2) The Tuoge supracrustal rocks and the Xingditage Group were derived from an immature source dominated by felsic igneous

rocks from a magmatic arc and then deposited at an active continental margin.

(3) The Tarim Craton recorded three early Precambrian crustal growth events with significant input of juvenile materials. The growth events occurred in the late Paleoarchean, the early Neoarchean and at the beginning of the Paleoproterozoic.

Acknowledgements

This study was supported by the National Basic Research Program of China (2014CB440801), the National Natural Science Foundation of China (41373034, 41173005, 41273012, and 41273048), the GIGCAS 135 project of the Guangzhou Institute of Geochemistry (Y234021001) and a grant of the State Key Laboratory of Isotope Geochemistry (SKLIG-RC-12-01). This is a contribution No. IS-2032 of GIGCAS and TIGER publication number 610.

Appendix A. Supplementary data

Supplementary data associated with this article can be found, in the online version, at http://dx.doi.org/10.1016/j.precamres.2015.01.008.

References

Andersen, T., 2002. Correction of common lead in U–Pb analyses that do not report ^{204}Pb. Chem. Geol. 192, 59–79.

BGMRX (Bureau of Geology Mineral Resources of Xinjiang Uygur Autonomous Region), 1993. Regional Geology of Xinjiang Uygur Autonomous Region, People's Republic of China. Geological Memoirs, Series 1, No. 32, Ministry of Geology and Mineral Resources, Geological Publishing House, Beijing, pp. 6–206 (in Chinese).

Bhat, M.I., Ghosh, S.K., 2001. Geochemistry of the 2.51 Ga old Rampur group pelites, western Himalayas: implications for their provenance and weathering. Precambrian Res. 108, 1–16.

Bhatia, M.R., Taylor, S.R., 1981. Trace-element geochemistry and sedimentary provinces: a study from the Tasman geosyncline, Australia. Chem. Geol. 33, 115–125.

Bhatia, M.R., 1983. Plate tectonics and geochemical composition of sandstones. J. Geol. 91, 611–627.

Bhatia, M.R., 1985. Rare earth element geochemistry of Australian Paleozoic graywackes and mudrocks: provenance and tectonic control. Sediment. Geol. 45, 97–113.

Bhatia, M.R., Crook, K.A.W., 1986. Trace element characteristics of graywackes and tectonic setting discrimination of sedimentary basins. Contrib. Mineral. Petrol. 92, 181–193.

Bouvier, A., Vervoort, J.D., Patchett, P.J., 2008. The Lu–Hf and Sm–Nd isotopic composition of CHUR: Constraints from unequilibrated chondrites and implications for the bulk composition of terrestrial planets. Earth Planet. Sci. Lett. 273 (1–2), 48–57.

Cao, X.F., Lü, X.B., Liu, S.T., Zhang, P., Gao, X., Chen, C., Mo, Y.L., 2011. LA-ICP-MS zircon dating, geochemistry, petrogenesis and tectonic implications of the Dapingliang Neoproterozoic granites at Kuluketage block, NW China. Precambrian Res. 186, 205–219.

Chu, N.C., Taylor, R.N., Chavagnae, V., Nesbitt, R.W., Boela, R.M., Milton, J.A., German, C.R., Bayon, G., Burton, K., 2002. Hf isotope ratio analysis using multi-collector inductively coupled plasma mass spectrometry: an evaluation of isobaric interference corrections. J. Anal. At. Spectrom. 17, 1567–1574.

Condie, K.C., 1993. Chemical composition and evolution of the upper continental crust: contrasting results from surface samples and shales. Chem. Geol. 104, 1–37.

Condie, K.C., 1998. Episodic continental growth and supercontinents: a mantle avalanche connection? Earth Planet. Sci. Lett. 163, 97–108.

Condie, K.C., 2000. Episodic continental growth models: afterthoughts and extensions. Tectonophysics 322, 153–162.

Condie, K.C., 2002. Breakup of a Paleopreoterozoic supercontinent. Gondwana Res. 5, 41–43.

Condie, K.C., Belousova, E., Griffin, W.L., Sircombe, K.N., 2009. Granitoid events in space and time: constraints from igneous and detrital zircon age spectra. Gondwana Res. 15, 228–242.

Condie, K.C., Bickford, M.E., Aster, R.C., Belousova, E., Scholl, D.W., 2011. Episodic zircon ages Hf isotopic composition, and the preservation rate of continental crust. Geol. Soc. Am. Bull. 123, 951–957.

Cox, R., Lowe, D.R., Cullers, R.L., 1995. The influence of sediment recycling and basement composition on evolution of mudrock chemistry in the southwestern United States. Geochim. Cosmochim. Acta 59, 2919–2940.

Cullers, R.L., 1994. The geochemical signatures of source rocks in size fractions of Holocene stream sediment derived from metamorphic rocks in the Wet Mountains region, USA. Chem. Geol. 113, 327–343.

Cullers, R.L., Podkovyrov, V.N., 2000. Geochemistry of the Mesoproterozoic Lakhanda shales in southeastern Yakutia Russia: implications for mineralogical and provenance control, and recycling. Precambrian Res. 104, 77–93.

Fedo, C.M., Nesbitt, H.W., Young, G.M., 1995. Unraveling the effects of potassium metasomatism in sedimentary rocks and paleosoils, with implications for paleoweathering conditions and provenance. Geology 23, 921–924.

Feng, B.Z., Zhou, Y.W., Peng, Q.M., Chi, S.F., Jiang, Q.G., Liu, Z.Y., Xing, L.X., Yang, T.Q., Ye, S.Q., 1995. Precambrian geology, precious and non-ferrous metal deposits in Kuruktag Area Xinjiang, Beijing. Geol. Publ. House, 1–88 (in Chinese with English abstract).

Floyd, P.A., Leveridge, B.E., 1987. Tectonic environment of the Devonian Gramscatho basin, south Cornwall: framework mode and geochemical evidence from turbiditic sandstones. J. Geol. Soc. Lond. 144, 531–542.

Gao, Z.J., Chen, J.L., Lu, S.N., Peng, C.W., Qin, Z.Y., 1993. The Precambrian Metamorphic Rocks. The Precambrian Geology No. 6 (in Chinese with English abstract).

GCRSX (Group for Compilation of Regional Stratigraphy of Xinjiang), 1981. Regional Stratigraphic Table of NW China: Xinjiang Uygur Autonomous Region Fascicule. Geological Publishing House, Beijing, pp. 496 (in Chinese with English abstract).

Ge, R.F., Zhu, W.B., Zheng, B.H., Wu, H.L., He, J.W., Zhu, X.Q., 2012. Early Pan-African magmatism in the Tarim Craton: insights from Zircon U–Pb–Lu–Hf isotope and geochemistry of granitoids in the Korla Area, NW China. Precambrian Res. 212–213, 117–138.

Ge, R.F., Zhu, W.B., Wu, H.L., He, J.W., Zheng, B.H., 2013. Zircon U–Pb ages and Lu–Hf isotopes of Paleoproterozoic metasedimentary rocks in the Korla Complex NW China: Implications for metamorphic zircon formation and geological evolution of the Tarim Craton. Precambrian Res. 231, 1–18.

Ge, R.F., Zhu, W.B., Wilde, S.A., Wu, H.L., He, J.W., Zheng, B.H., 2014a. Archean magmatism and crustal evolution in the northern Tarim Craton: Insights from zircon U–Pb–Hf–O isotopes and geochemistryof ~2.7 Ga orthogneiss and amphibolite in the Korla Complex. Precambrian Res. 252, 145–165.

Ge, R.F., Zhu, W.B., Wilde, S.A., He, J.W., 2014b. Zircon U–Pb–Lu–Hf–O isotopic evidence for ≥3.5 Ga crustal growth, reworking and differentiation in the northern Tarim Craton. Precambrian Res., http://dx.doi.org/10.1016/j.precamres.2014.05.004.

Geraldes, M.C., Van Schmus, W.R., Condie, K.C., Bell, S., Teixeira, W., Babinski, M., 2001. Proterozoic geologic evolution of the SW part of the Amazonian Craton in Mato Grosso state, Brazil. Precambrian Res. 111, 91–128.

Griffin, W.L., Wang, X., Jackson, S.E., Pearson, N.J., O'Reilly, S.Y., Xu, X., Zhou, X., 2002. Zircon chemistry and magma mixing, SE China: in-situ analysis of Hf isotopes. Tonglu and Pingtan igneous complexes. Lithos 61, 237–269.

Griffin, W.L., Belousova, E.A., Shee, S.R., Pearson, N.J., O'Reilly, S.Y., 2004. Archaean crustal evolution in the northern Yilgarn Craton: U–Pb and Hf isotope evidence from detrital zircons. Precambrian Res. 131, 231–282.

Guo, Z.J., Zhang, Z.C., Liu, S.W., Li, H.M., 2003. U–Pb geochronological evidence for the early Precambrian complex of the Tarim Craton, NW China. Acta Petrologica Sin. 19 (3), 537–542.

Guo, Z.J., Yin, A., Robinson, A., Jia, C.Z., 2005. Geochronology and geochemistry of deep-drill-core samples from the basement of the central Tarim basin. J. Asian Earth Sci. 25 (1), 45–56.

He, Y.H., Zhao, G.C., Sun, M., Xia, X.P., 2009. SHRIMP and LA-ICP-MS zircon geochronology of the Xiong'er volcanic rocks: implications for the Paleo-Mesoproterozoic evolution of the southern margin of the North China Craton. Precambrian Res. 168, 213–222.

He, Y.H., Zhao, G.C., Sun, M., Han, Y., 2010. Petrogenesis and tectonic setting of volcanic rocks in the Xiaoshan and Waifangshan areas along the southern margin of the North China Craton: constraints from bulk-rock geochemistry and Sr–Nd isotopic composition. Lithos 114, 186–199.

He, Z.Y., Zhang, Z.M., Zhong, K.Q., Wang, W., Santosh, M., 2012. Neoproterozoic granulites from the northeastern margin of the Tarim Craton: Petrology, zircon U–Pb ages and implications for the Rodinia assembly. Precambrian Res. 212–213, 21–33.

Hoskin, P.W.O., Schaltegger, U., 2003. The composition of zircon and igneous and Metamorphic petrogenesis. In: Hanchar, J.M, Hoskin, P.W.O. (Eds.), Zircon. Rev. Miner. Geochem. 53, 27–62.

Hou, G.T., Santosh, M., Qian, X.L., Lister, G.S., Li, J.H., 2008. Configuration of the Late Paleoproterozoic supercontinent Columbia: insights from radiating mafic dyke swarms. Gondwana Res. 14, 395–409.

Hu, A.Q., Rogers, G., 1992. Discovery of 3.3 Ga Archaen rocks in north Tarim Block of Xinjiang, western China. Chin. Sci. Bull. 37, 1546–1549.

Hu, A.Q., Wang, Z.G., Tu, G.Z., 1997. Geological Evolution and Diagenic and Metallogenetic Regularity in Northern Xinjiang. Science Press, Beijing (in Chinese).

Hu, A.Q., Jahn, B.M., Zhang, G.X., Chen, Y.B., Zhang, Q.F., 2000. Crustal evolution and Phanerozoic crustal growth in northern Xinjiang: Nd isotope evidence 1. Isotopic characterization of basement rocks. Tectonophysics 328, 15–51.

Huang, Z.Y., Long, X.P., Kröner, A., Yuan, C., Wang, Q., Sun, M., Zhao, G.C., Wang, Y.J., 2013. Geochemistry, zircon U–Pb ages and Lu–Hf isotopes of early Paleozoic plutons in the northwestern Chinese Tianshan: Petrogenesis and geological implications. Lithos 182–183, 48–66.

Kamp, P.C., Leake, B.E., 1985. Petrography and geochemistry of feldspathic and mafic sediments of the northeastern Pacific margin. Trans. R. Soc. Edinburgh: Earth Sci. 76, 411–499.

Karlstrom, K.E., Harlan, S.S., Åhäll, K.I., Williams, M.L., McLelland, J., Geissman, J.W., 2001. Long-lived (18–1.0 Ga) convergent orogen in southern Laurentia,

its extensions to Australia and Baltica, and implications for refining Rodinia. Precambrian Res. 111, 5–30.
Lei, R.X., Wu, C.Z., Chi, G.X., Chen, G., Gu, L.X., Jiang, Y.H., 2012. Petrogenesis of the Palaeoproterozoic Xishankou pluton, northern Tarim block, northwest China: implications for assembly of the supercontinent Columbia. Int. Geol. Rev. 54, 1829–1842.
Li, H.M., Lu, S.N., Zheng, J.K., Yu, H.F., Zhao, F.Q., Li, H.K., Zou, Y.C., 2001. Dating of 3.6 Ga zircons in granite-gneiss from the Eastern Altyn Mountains and Its Geological Significance. Bulletin of Mineralogy, Petrology and Geochemistry 20, 259–262.
Liu, Y.S., Xin, H.T., Zhou, S.J., Teng, X.J., Yang, J.Q., Lv, H.Q., 2010. Precambrian to Paleozoic Tectonic Evolution in the Lapeiquan Area, Eastern Altyn Tage. Geological Publishing House, Beijing, pp. 211.
Long, X.P., Yuan, C., Sun, M., Zhao, G.C., Xiao, W.J., Wang, Y.J., Yang, Y.H., Hu, A.Q., 2010. Archean crustal evolution of the northern Tarim Craton NW China: Zircon U–Pb and Hf isotopic constraints. Precambrian Res. 180, 272–284.
Long, X.P., Yuan, C., Sun, M., Xiao, W.J., Zhao, G.C., Zhou, K.F., Wang, Y.J., Hu, A.Q., 2011a. The discovery of the oldest rocks in the Kuluketage area and its geological implications. Sci. China: Earth Sci. 54, 342–348.
Long, X.P., Yuan, C., Sun, M., Kröner, A., Zhao, G.C., Wilde, S., Hu, A.Q., 2011b. Reworking of the Tarim Craton by underplating of mantle plume-derived magmas: Evidence from Neoproterozoic granitoids in the Kuluketage area NW China. Precambrian Res. 187, 1–14.
Long, X.P., Sun, M., Yuan, C., Kröner, A., Hu, A.Q., 2012a. Zircon REE patterns and geochemical characteristics of Paleoproterozoic anatectic granite in the northern Tarim Craton NW China: implications for the reconstruction of the Columbia supercontinent. Precambrian Res. 222–223, 474–487.
Long, X.P., Yuan, C., Sun, M., Safonova, I., Xiao, W.J., Wang, Y.J., 2012b. Geochemistry and U–Pb detrital zircon dating of Paleozoic graywackes in East Junggar NW China: Insights into subduction-accretion processes in the southern Central Asian Orogenic Belt. Gondwana Res. 21, 637–653.
Long, X.P., Yuan, C., Sun, M., Kröner, A., Zhao, G.C., 2014. New geochemical and combined zircon U–Pb and Lu–Hf isotopic data of orthogneisses in the northern Altyn Tagh, northern margin of the Tibetan plateau: implication for Archean evolution of the Dunhuang Block and crust formation in NW China. Lithos 200–201, 418–431.
Lu, S.N., Yuan, G.B., 2003. Geochronology of early Precambrian magmatic activities in Aketasdhtage East Altyn tagh. Acta Geol. Sin. 77, 61–68 (in Chinese with English abstract).
Lu, S.N., Li, H.K., Zhang, C.L., Niu, G.H., 2008. Geological and geochronological evidence for the Precambrian evolution of the Tarim Craton and surrounding continental fragments. Precambrian Res. 160, 94–107.
Machado, N., Simonetti, A., 2001. U–Pb dating and Hf isotopic composition of zircon by laser ablation-MC-ICP-MS. In: In Laser Ablation-ICPMS in the Earth Sciences. Short Course, vol. 29. Mineralogical Association of Canada, Ottawa, pp. 121–146.
McLennan, S.M., 1989. Rare earth elements in sedimentary rocks: influence of provenance and sedimentary processes. Rev. Mineral. Geochem. 21, 169–200.
McLennan, S.M., Taylor, S.R., McCulloch, M.T., Maynard, J.B., 1990. Geochemical and Nd–Sr isotopic composition of deep-sea turbidites: crustal evolution and plate tectonic associations. Geochim. Cosmochim. Acta 43, 375–388.
McLennan, S.M., Hemming, S., McDaniel, D.K., Hanson, G.N., 1993. Geochemical approaches to sedimentation, provenance, and tectonics. Geol. Soc. Am. Special Paper 284, 21–40.
Nesbitt, H.W., Young, G.M., 1982. Early Proterozoic climates and plate motions inferred from major element chemistry of lutites. Nature 199, 715–717.
Nesbitt, H.W., Young, G.M., 1984. Prediction of some weathering trends of plutonic and volcanic rocks based on thermodynamics and kinetic considerations. Geochim. Cosmochim. Acta 48, 1523–1534.
RGS (Regional Geological Survey of Xinjiang Geological Bureau), 1965. 1:200,000 Geological Map and Report of Xinger. Geological Publishing House, Beijing (in Chinese).
Roser, B.P., Korsch, R.J., 1986. Determination of tectonic setting of sandstone-mudstone suites using SiO_2 content and K_2O/Na_2O ratio. J. Geol. 94, 635–650.
Rogers, J.J.W., Santosh, M., 2002. Configuration of Columbia, a Mesoproterozoic supercontinent. Gondwana Res. 5, 5–22.
Santosh, M., 2010. Assembling North China Craton within the Columbia supercontinent: the role of double-sided subduction. Precambrian Res. 178, 149–167.
Shu, L.S., Deng, X.L., Zhu, W.B., Ma, D.S., Xiao, W.J., 2011. Precambrian tectonic evolution of the Tarim Block, NW China: new geochronological insights from the Quruqtagh domain. J. Asian Earth Sci. 42, 774–790.
Söderlund, U., Patchett, P.J., Vervoort, J.D., Isachsen, C.E., 2004. The ^{176}Lu decay constant determined by Lu–Hf and U–Pb isotope systematics of Precambrian mafic intrusions. Earth Planet. Sci. Lett. 219, 311–324.
Stein, M., Hofmann, A.W., 1994. Mantle plumes and episodic crustal growth. Nature 372, 63–68.
Sun, S.-S., McDonough, W.F., 1989. Chemical and isotopic systematics of oceanic basalts: implications for mantle composition and processes. In: Saunders, A.D., Norry, M.J. (Eds.), Magmatism in the Ocean Basin, 42. Geological Society Special Publication, Blackwell Scientific Publications, Oxford, pp. 313–346.
Taylor, S.R., McLennan, S.M., 1985. The Continental Crust: Its Composition and Evolution. Blackwell Scientific Publications, Oxford, UK, pp. 312.
Wang, C.Y., Campbell, I.H., Allen, C.M., Williams, I.S., Eggins, S.M., 2009. Rate of growth of the preserved North American continental crust: evidence from Hf and O isotopes in Mississippi detrital zircons. Geochim. Cosmochim. Acta 73, 712–728.
Wilde, S.A., Zhao, G., Sun, M., 2002. Development of the North China Craton during the Late Archaean and its final amalgamation at 1.8 Ga: some speculations on its position within a global Palaeoproterozoic Supercontinent. Gondwana Res. 5, 85–94.
Wu, C.Z., Santosh, M., Chen, Y.J., Samson, I.M., Lei, R.X., Dong, L.H., Qu, X., Gu, L.X., 2014. Geochronology and geochemistry of Early Mesoproterozoicmeta-diabase sills from Quruqtagh in the northeastern Tarim Craton: Implications for breakup of the Columbia supercontinent. Precambrian Res. 241, 29–43.
Xia, X.P., Sun, M., Geng, H., Sun, Y., Wang, Y., Zhao, G.C., 2011. Quasi-simultaneous determination of U–Pb and Hf isotope compositions of zircon by excimer laser-ablation multiple-collector ICPMS. J. Anal. At. Spectrom. 26, 1868–1871.
Xu, B., Jian, P., Zheng, H.F., Zhou, H.B., Zhang, L.F., Liu, D.Y., 2005. U–Pb zircon geochronology and creochemistry of Neoproterozoic volcanic rocks in the Tarim Block of northwest China: implications for the breakup of Rodinia supercontinent and Neoproterozoic glaciations. Precambrian Res. 136, 107–123.
Xu, B., Xiao, S.H., Zou, H.B., Chen, Y., Li, Z.-X., Song, B., Liu, D.Y., Zhou, C.M., Yuan, X.L., 2009. SHRIMP zircon U–Pb age constraints on Neoproterozoic Quruqtagh diamictites in NW China. Precambrian Res. 168, 247–258.
Xu, Z.Q., He, B.Z., Zhang, C.L., Zhang, J.X., Wang, Z.M., Cai, Z.H., 2013. Tectonic framework and crustal evolution of the Precambrian basement of the Tarim Block in NW China: new geochronological evidence from deep drilling samples. Precambrian Res. 235, 150–162.
Yang, J., Gao, S., Chen, C., Tang, Y., Yuan, H., Gong, H., Xie, S., Wang, J., 2009. Episodic crustal growth of North China as revealed by U–Pb age and Hf isotopes of detrital zircons from modern rivers. Geochim. Cosmochim. Acta 73, 2660–2673.
Yang, R.D., Luo, X.R., Zhang, C.L., Tian, J.Q., Bao, Y.F., 2010. Sedimentation characteristic and carbon isotopic composition in late Paleoproterozoic Xingditage Group in Quruqtagh region of Xinjiang, China. Northwestern Geol. 43 (1), 36–43 (in Chinese with English abstract).
Yuan, C., Zhou, M.F., Sun, M., Zhao, Y.J., Wilde, S., Long, X.P., Yan, D.P., 2010. Triassic granitoids in the eastern Songpan Ganzi Fold Belt SW China: magmatic response to geodynamics of the deep lithosphere. Earth Planet. Sci. Lett. 290, 481–492.
Zhang, C.L., Li, Z.X., Li, X.H., Yu, H.F., Ye, H.M., 2007a. An early Paleoproterozoic high-K intrusive complex in southwestern Tarim Block NW China: age, geochemistry, and tectonic implications. Gondwana Res. 12, 101–112.
Zhang, C.L., Li, X.H., Li, Z.X., Lu, S.N., Ye, H.M., Li, H.M., 2007b. Neoproterozoic ultramafic–mafic-carbonatite complex and granitoids in Quruqtagh of northeastern Tarim Block, western China: geochronology, geochemistry and tectonic implications. Precambrian Res. 152, 149–169.
Zhang, C.L., Li, Z.X., Li, X.H., Ye, H.M., 2009. Neoproterozoic mafic dyke swarms at the northern margin of the Tarim Block, NW China: age, geochemistry, petrogenesis and tectonic implications. J. Asian Earth Sci. 35, 167–179.
Zhang, C.L., Yang, D.S., Wang, H.Y., Takahashi, Y., Ye, H.M., 2011. Neoproterozoic mafic-ultramafic layered intrusion in Quruqtagh of northeastern Tarim Block NW China: two phases of mafic igneous activity with different mantle sources. Gondwana Res. 19, 177–190.
Zhang, C.L., Li, H.K., Santosh, M., Li, Z.X., Zou, H.B., Wang, H.Y., Ye, H.M., 2012a. Precambrian evolution and cratonization of the Tarim Block, NW China: petrology, geochemistry Nd-isotopes and U–Pb zircon geochronology from Archaean gabbro-TTG–potassic granite suite and Paleoproterozoic metamorphic belt. J. Asian Earth Sci. 47, 5–20.
Zhang, J.X., Yu, S.Y., Gong, J.H., Li, H.K., Hou, K.J., 2012b. ~1.85 Ga HP granulite facies metamorphism in the Dunhuang block of the Tarim Craton NW China: evidence from zircon U–Pb datings of mafic granulites. J. Geol. Soc. 169, 511–514.
Zhang, C.L., Zou, H.B., Li, H.K., Wang, H.Y., 2013a. Tectonic framework and evolution of the Tarim Block in NW China. Gondwana Res. 23, 1306–1315.
Zhang, J.X., Yu, S.Y., Gong, J.H., Li, H.K., Hou, K.J., 2013b. The latest Neoarchean–Paleoproterozoic evolution of the Dunhuang block, eastern Tarim Craton, northwestern China: evidence from zircon U–Pb dating and Hf isotopic analyses. Precambrian Res. 226, 21–42.
Zhang, C.L., Zou, H.B., Santosh, M., Ye, X.T., Li, H.K., 2014. Is the Precambrian basement of the Tarim Craton in NW China composed of discrete terranes? Precambrian Res. 254, 226–244.
Zhao, G.C., Sun, M., Wilde, S.A., 2002. Review of global 2.1–1.8 Ga orogens: implications for a Pre-Rodinia supercontinent. Earth-Sci. Rev. 59, 125–162.
Zhao, G.C., Sun, M., Wilde, S.A., Li, S.Z., 2004. A Paleo-Mesoproterozoic supercontinent: assembly, growth and breakup. Earth-Sci. Rev. 67, 91–123.
Zhao, G.C., Sun, M., Wild e, S.A., Li, S.Z., 2005. Late Archean to Paleoproterozoic evolution of the North China Craton: key issues revisited. Precambrian Res. 136, 177–202.
Zhao, G.C., He, Y.H., Sun, M., 2009. The Xiong'er volcanic belt at the southern margin of the North China Craton: Petrographic and geochemical evidence for its outboard position in the Paleo-Mesoproterozoic Columbia Supercontinent. Gondwana Res. 16, 170–181.
Zhao, G.C., Cawood, P.A., 2012. Precambrian geology of China. Precambrian Res. 222–223, 13–54.
Zhu, W.B., Zheng, B.H., Shu, L.S., Ma, D.S., Wu, H.L., Li, Y.X., Huang, W.T., Yu, J.J., 2011a. Neoproterozoic tectonic evolution of the Precambrian Aksu blueschist terrane, northwestern Tarim, China: insights from LA-ICP-MS zircon U–Pb ages and geochemical data. Precambrian Res. 185, 215–230.
Zhu, W.B., Zheng, B.H., Shu, L.S., Ma, D.S., Wan, J.L., Zheng, D.W., Zhang, Z.Y., Zhu, X.Q., 2011b. Geochemistry and SHRIMP U–Pb zircon geochronology of the Korla mafic dykes: constrains on the Neoproterozoic continental breakup in the Tarim Block, northwest China. J. Asian Earth Sci. 42, 791–804.
Zong, K.Q., Liu, Y.S., Zhang, Z.M., He, Z.Y., Hu, Z.C., Guo, J.L., Chen, K., 2013. The generation and evolution of Archean continental crust in the Dunhuang block, northeastern Tarim craton, northwestern China. Precambrian Res. 235, 251–263.